Published in final edited form as:

Cell. 2019 December 12; 179(7): 1566–1581.e16. doi:10.1016/j.cell.2019.11.022.

A Translation-Activating Function of MIWI/piRNA during Mouse Spermiogenesis

Peng Dai[#1], **Xin Wang**[#1], **Lan-Tao Gou**[#1,2], **Zhi-Tong Li**[#1], **Ze Wen**[#1], **Zong-Gui Chen**[#3], **Min-Min Hua**[1,4], **Ai Zhong**[1], **Lingbo Wang**[4,5], **Haiyang Su**[6], **Huida Wan**[7], **Kun Qian**[6], **Lujian Liao**[7], **Jinsong Li**[5,8], **Bin Tian**[9], **Dangsheng Li**[1], **Xiang-Dong Fu**[2], **Hui-Juan Shi**[4,*], **Yu Zhou**[3,*], **Mo-Fang Liu**[1,8,10,*]

[1]State Key Laboratory of Molecular Biology, Shanghai Key Laboratory of Molecular Andrology, CAS Center for Excellence in Molecular Cell Science, Shanghai Institute of Biochemistry and Cell Biology, Chinese Academy of Sciences-University of Chinese Academy of Sciences, Shanghai 200031, China

[2]Department of Cellular and Molecular Medicine, University of California, San Diego, La Jolla, CA 92093-0651, USA

[3]College of Life Sciences, Institute of Advanced Studies, Wuhan University, Wuhan, Hubei 430072, China

[4]NHC Key Lab of Reproduction Regulation (Shanghai Institute of Planned Parenthood Research), Pharmacy School, Fudan University, Shanghai, 200032, China

[5]State Key Laboratory of Cell Biology, Shanghai Institute of Biochemistry and Cell Biology, Chinese Academy of Sciences-University of Chinese Academy of Sciences, Shanghai 200031, China

[6]School of Biomedical Engineering, Med-X Research Institute, Shanghai Jiao Tong University, Shanghai 200030, China

[7]Shanghai Key Laboratory of Regulatory Biology and Shanghai Key Laboratory of Brain Functional Genomics, School of Life Sciences, East China Normal University, Shanghai 200241, China

[8]School of Life Science and Technology, Shanghai Tech University, Shanghai 201210, China

[9]Department of Microbiology, Biochemistry and Molecular Genetics, Rutgers New Jersey Medical School, Newark, New Jersey 07103, USA

[10]Lead Contact

[*]Correspondence: shihuijuan@sippr.stc.sh.cn (H.-J.S.), yu.zhou@whu.edu.cn (Y.Z.), mfliu@sibcb.ac.cn (M.-F.L.).

AUTHOR CONTRIBUTIONS

M.-F.L., Y.Z., and H.-J.S. planned the project. P.D., X.W., K.Q., L.L., J.L., B.T., D.L., X.-D.F., H.-J.S., Y.Z., and M.-F.L. designed the experiments. P.D., X.W., L.-T.G., Z.-T.L., Z.W., M.-M.H., A.Z., L.W., H.S., and H.W. conducted the experiments. P.D., Z.-G.C., Y.Z., and M.-F.L. analyzed the data. P.D., X.-D.F., and M.-F.L. wrote the paper. All authors discussed the results and commented on the manuscript. M.-F.L. supervised the overall work, and Y.Z. was responsible for Bioinformatics studies.

SUPPLEMENTAL INFORMATION

Supplemental Information can be found online at https://doi.org/10.1016/j.cell.2019.11.022.

DECLARATION OF INTERESTS

The authors declare no competing interests.

[#] These authors contributed equally to this work.

SUMMARY

Spermiogenesis is a highly orchestrated developmental process during which chromatin condensation decouples transcription from translation. Spermiogenic mRNAs are transcribed earlier and stored in a translationally inert state until needed for translation; however, it remains largely unclear how such repressed mRNAs become activated during spermiogenesis. We previously reported that the MIWI/piRNA machinery is responsible for mRNA elimination during late spermiogenesis in preparation for spermatozoa production. Here we unexpectedly discover that the same machinery is also responsible for activating translation of a subset of spermiogenic mRNAs to coordinate with morphological transformation into spermatozoa. Such action requires specific base-pairing interactions of piRNAs with target mRNAs in their 3′ UTRs, which activates translation through coupling with *cis*-acting AU-rich elements to nucleate the formation of a MIWI/piRNA/eIF3f/HuR super-complex in a developmental stage-specific manner. These findings reveal a critical role of the piRNA system in translation activation, which we show is functionally required for spermatid development.

In Brief

The piRNA pathway, through functional interplay with HuR and eIF3f, plays an important role in translational activation of a specific set of mRNAs during mouse spermiogenesis.

Graphical Abstract

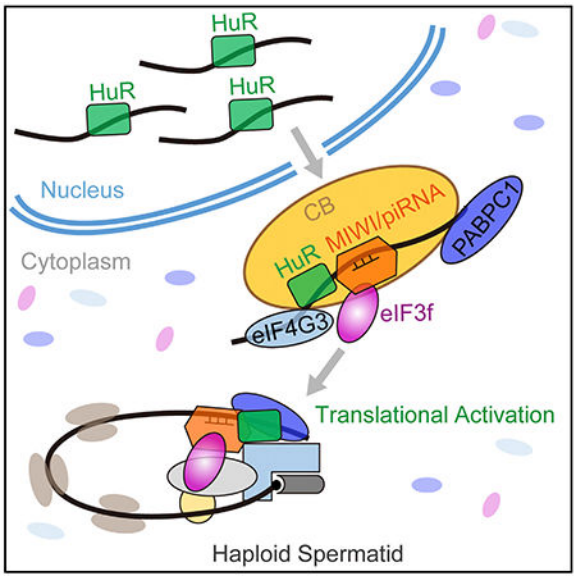

INTRODUCTION

The post-meiotic phase of male germ cell development in mammals undergoes a series of dramatic morphological changes, including acrosome and flagellum formation, nuclear condensation, and cytoplasmic exclusion, which are driven by a highly regulated sequence

of biochemical reactions (Yan, 2009; Meistrich and Hess, 2013). This differentiation process, called spermiogenesis, consists of at least 16 sequential transition steps in mice, which occur from postpartum day 21 to 28 for round spermatid differentiation (steps 1–8), postpartum day 28–35 for morphological transformation into elongating spermatids (steps 9–11), elongated or condensed spermatids (steps 12–14), and finally spermatozoa (steps 15–16) (Yan, 2009; Meistrich and Hess, 2013). These sequential transitions are programmed by a series of highly orchestrated regulatory events in gene expression at each developmental step. Due to chromatin compaction during the course of spermatid elongation, transcription becomes gradually inhibited during spermiogenesis before ceasing completely later on (Steger, 1999; Sassone-Corsi, 2002). Thus, the program of spermiogenesis relies on gene products that are transcribed earlier and stored in translationally inert messenger ribonucleoproteins (mRNPs) until needed for translation (Steger, 1999; Sassone-Corsi, 2002). This phenomenon, known as uncoupling between transcription and translation, is a unique feature of gene regulation during spermiogenesis, which has been one of the major mysteries in understanding the germ cell development program.

The evolutionarily conserved PIWI family proteins have been well documented for their essential roles in germline development and gametogenesis on various animal models (Siomi et al., 2011; Iwasaki et al., 2015). Most recently, we showed a causative role of human *Piwi* (*Hiwi*) mutations in male infertility, establishing a definitive linkage of human *Piwi* genes to human infertility (Gou et al., 2017; Hasuwa et al., 2018). PIWI proteins are known to enlist germline-specific PIWI-interacting RNAs (piRNAs), whose primary function has been thought to silence transposable elements, thereby protecting the genome integrity in animal germ cells (Siomi et al., 2011; Iwasaki et al., 2015). Importantly, we and others demonstrated that the PIWI/piRNA machinery also mediates the degradation of mRNA transcripts via miRNA- and/or siRNA-like mechanisms in germ cells (Gou et al., 2014; Zhang et al., 2015; Goh et al., 2015; Watanabe et al., 2015; Vourekas et al., 2016; Shen et al., 2018; Zhang et al., 2018). These findings demonstrate that the piRNA system also regulates protein-coding genes beyond silencing transposable elements in germ cells.

To understand the mechanism for the PIWI/piRNA machinery to regulate spermiogenic mRNAs at post-transcriptional levels, we previously embarked on a systematic effort to identify mouse PIWI (MIWI)-associated mRNAs in mouse spermatids by RNA co-immunoprecipitation (RIP) in combination with UV crosslinking coupled with deep sequencing (CLIP-seq) and found that nearly all mRNAs in complex with MIWI could be matched to a specific set of piRNAs (Gou et al., 2014; Zhang et al., 2015). Using a mouse spermatocyte-derived GC-2spd(ts) cell line (Hofmann et al., 1995) as a cell-culture model, we determined the functional consequence of predicted piRNA:mRNA pairs on a 3′ UTR-based reporter system in response to individual synthetic piRNAs. While this cell line is unlikely to perfectly recapitulate PIWI/piRNA function during spermiogenesis, it is the only cell-culture model that we found to be functional for biochemical studies because piRNAs, MIWI, MILI, and Tudor proteins as well as MIWI/piRNA complexes are all present (Gou et al., 2014). Indeed, on this cellular model, we found that many tested piRNAs are able to induce downregulation of their cognate targets (Gou et al., 2014; Zhang et al., 2015).

During this analysis, we were surprised to note that among the predicted piRNA:mRNA pairs (~100) that we tested, five such targets (i.e., *Plectin, Agfg1, Tbpl1, Cnot4*, and *Atg12*) were instead activated by their cognate piRNAs. All of these piRNA-activated targets are characterized by AU-rich elements (AREs) in their 3′ UTRs, which we show are required for piRNA-mediated translational activation. Pursuing this unexpected regulatory paradigm, we uncover the involvement of the ARE-binding protein HuR and the translation initiation factor eIF3f in mediating translation activation of these MIWI/piRNA targets. Focusing on *Agfg1* and *Tbpl1*, the two genes critical for acrosome formation during spermatid development (Kang-Decker et al., 2001; Zhang et al., 2001), we demonstrate that their activation by the piRNA system is indeed indispensable for acrosome formation in spermatozoa. These findings, coupled with the established role of MIWI/piRNA in massive mRNA degradation for inactivating vast cellular programs in preparation for spermatozoa production from spermatids, unveil a dual function of the MIWI/piRNA machinery in differential regulation of its target mRNAs in spermatids to instruct post-meiotic male germ cell development in mice.

RESULTS

piRNAs Activate Target mRNAs via Imperfect Base-Pairing Interactions

Our previous studies showed that the MIWI complex in mouse spermatids harbors both piRNAs and mRNAs and that most tested piRNAs repress mRNA targets via a base-pairing rule using a 3′ UTR-based reporter screen system in transfected GC-2spd(ts) cells (Gou et al., 2014). Surprisingly, we found that five specific piRNAs (i.e., piR_1029, piR_3146, piR_2617, piR_010111, and piR_3344) significantly upregulated their cognate target reporters *Plectin, Agfg1, Tbpl1, Cnot4*, and *Atg12* (Figures 1A and 1B). None of these piRNAs caused any measurable change in reporter mRNA expression (Figure 1C), implying a function of piRNAs at the level of translation. We were particularly attracted to this possibility, as it would suggest a potential role of piRNAs in selective translation activation in mouse spermatids, which has been one of the major mysteries in understanding spermiogenesis.

We next asked whether specific piRNA:mRNA pairing is required for this newly discovered piRNA function. To this end, we constructed mutant reporters in each with deletion of the 7~8-nt (nucleotide) sequence complementary to the 5′ part of the corresponding piRNAs and also synthesized mutant piRNAs to substitute the 7~8-nt sequence in each with complementary nucleotides (Figure 1A). We found that both deletion of piRNA-binding sites in the reporters and mutations in the corresponding piRNAs completely abolished the activation effect of piRNAs (Figure 1B), again without detectable impact on reporter mRNA levels (Figure 1C). This supports the requirement of piRNA:mRNA base pairing for piRNA-induced target activation. Moreover, in agreement with recent observations in *C. elegans* (Shen et al., 2018; Zhang et al., 2018), we found that one mismatch in the piR_1029:*Plectin* mRNA pairing region is sufficient to disrupt the piRNA function (Figure S1A), further demonstrating the indispensability of piRNA:mRNA base pairing for this new piRNA function.

Consistent with the possibility of translation activation, our sucrose gradient analysis showed that, relative to the piR_1029 (Mut) control, co-transfected piR_1029 significantly elevated the association of MIWI with the reporter mRNA in the polysome fractions, which was accompanied with a reduction in lighter RNP fractions (Figures S1B–S1D). These results confirm an active role of piRNA:mRNA base pairing in trafficking more target transcripts to the translation machinery, providing initial evidence for piRNA-dependent translation activation of target mRNAs through imperfect base pairing in the 3′ UTRs.

MIWI Is Required for piRNA-Mediated Translation Activation

To determine whether MIWI is required for piRNA-induced target activation, we took advantage of our previous MIWI CLIP data generated on enriched mouse spermatids (Gou et al., 2014; Zhang et al., 2015), showing clusters of specific MIWI-CLIP tags on cognate piRNA target sites on *Plectin, Agfg1, Tbpl1, Cnot4*, and *Atg12* mRNAs (Figure 2A), thus pinpointing specific MIWI-binding sites in these mRNAs *in vivo*. To further substantiate these observations, we performed RIP and found that Flag-MIWI readily pulled down the *Plectin* reporter mRNA in piR_1029, but not piR_1029 (Mut) co-transfected GC-2spd(ts) (Figure S2A), indicating that specific piRNA:mRNA base pairing guides MIWI loading onto its targeted mRNA.

We next co-transfected *Miwi* siRNA (*Miwi* siR) to knock down endogenous *Miwi* in GC-2spd(ts) cells. We found that MIWI depletion abrogated the effect of piR_1029 on the *Plectin* reporter (Figure 2B). In contrast, depletion of either MILI (another mouse Piwi protein expressed in GC-2spd(ts) cells) or AGO2 (a key component of the microRNA/small interfering RNA [miRNA/siRNA] machinery) showed little impact on piRNA-induced target activation (Figure S2B). Conversely, ectopic expression of Flag-MIWI further enhanced the activation effect of piR_1029 on the *Plectin* reporter (Figure 2C). Neither *Miwi* knockdown nor overexpression altered the reporter mRNA expression (Figures S2C and S2D). These results indicate the functional requirement of MIWI for piRNA-induced target activation.

To further substantiate this piRNA-guided MIWI function in translation activation, we determined whether its piRNA loading capacity is required. We employed a *Miwi* siRNA to deplete endogenous MIWI in GC-2spd(ts) cells and then complemented the cells with either Flag-tagged wild-type human PIWI (HIWI) or its piRNA loading-deficient Y345/346A mutant (Figure 2D). As expected, wild-type HIWI was able to restore the piR_1029-dependent reporter activation in MIWI-depleted GC-2spd(ts) cells, but the Y345/346A mutant failed to rescue, demonstrating that the piRNA-loading ability of PIWI is indispensable for piRNA-mediated target activation. This further supports the functional requirement of MIWI in this newly discovered piRNA function.

Identification of eIF3f as a Key Partner of MIWI in Translation Activation

To understand the mechanism, we next aimed to identify a potential cofactor(s) with the MIWI/piRNA machinery to activate target mRNA translation. To this end, we carried out a yeast two-hybrid screen to search for candidate MIWI-interacting proteins, paying particular attention to hits with links to translation using mouse testis and human fetal brain cDNA libraries. The f-subunit of eukaryotic translation initiation factor 3 (eIF3f) stood out from the

screen as a potent MIWI-interacting protein, as 37 out of 71 positive clones all contained *eIF3f* cDNA (Table S1). We confirmed the interaction between MIWI and eIF3f by co-immunoprecipitation (coIP) in both co-transfected 293T cells (Figure 3A) and mouse testes (Figure 3B). In addition, we found that MIWI was also able to pull down eIF3a and eIF3c, two other eIF3 core subunits, in mouse testes (Figure 3B). Furthermore, unbiased proteomic analysis of anti-MIWI IPed complexes from mouse testes identified eIF3a, eIF3b, eIF3c, eIF3e, eIF3f, eIF3h, eIF3l, and eIF3m (see Figure S3H). These findings suggest that MIWI may recruit the entire eIF3 complex via eIF3f in mouse testes.

We next performed the GST pull-down assay using purified recombinant GST-eIF3f and *in vitro* translated [^{35}S]Met-MIWI, showing the direct interaction between them (Figure 3C). Such an interaction was barely affected in response to treatment with RNase A (Figure 3B) or in the presence of piRNA (Figure S2E), indicating that RNA is not required for the MIWI-eIF3f interaction. Importantly, knockdown of eIF3f in GC-2spd(ts) cells completely attenuated the effect of piR_1029 on the *Plectin* reporter (Figure 3D), whereas the ectopic expression of Flag-eIF3f further strengthened the impact of piR_1029 on the reporter activity (Figure 3E). Neither *eIF3f* knockdown nor overexpression altered the reporter mRNA level (Figure S2F). The data strongly suggested an essential role of eIF3f in piRNA-induced translation activation. Of note, eIF3f has been shown as a nonessential eukaryotic initiation subunit, which appears to function in a tissue-specific or intracellular and signaling context-dependent manner (Marchione et al., 2013). Indeed, our high-resolution sucrose gradient analysis revealed that *eIF3f* knockdown caused little, if any, alteration in the polysome-to-monosome (P/M) ratio in GC-2spd(ts) cells (Figure S2G), suggesting that eIF3f is not essential for global mRNA translation in these cells. These data point to a specific function of eIF3f in piRNA-activated translation.

AU-Rich Elements in 3′ UTR Are Responsible for piRNA-Induced Target Activation

We next investigated how the MIWI/piRNA complex induces mRNA decay in the vast majority of target transcripts while activating translation of a subset. Given the established roles of *cis*-elements in the 3′ UTRs in regulating mRNA metabolism in male germ cells (Kleene, 2013), we hypothesized that certain specific *cis*-elements in the 3′ UTRs might be responsible for differentiating translation activation and mRNA degradation by the piRNA system. Close inspection of the five validated piRNA-activated targets revealed AREs in their 3′ UTRs (Figure S3A), and indeed, mutations in the AREs abolished the activation effect of piRNAs on the reporters (Figure 4A). These observations suggest that AREs in the 3′ UTRs may be a critical sequence feature for piRNA-mediated translation activation.

To further test whether an ARE is sufficient to trigger piRNA-induced translation activation, we inserted an ARE into the *Grk4* 3′ UTR reporter, a target to be repressed by piR_010111 (Gou et al., 2014), and to additionally test potential position-sensitive effects, we inserted the ARE at 550 nt, 950 nt, 1,350 nt, or 1,750 nt downstream of the piRNA-binding site, respectively (Figure 4B, left). An ARE at 1,350 nt, but not other locations, successfully reversed the repressive effect of piR_010111 to activation on the reporter (Figure 4B, middle). These results indicate that an ARE is sufficient to enable piRNA-mediated target activation in a position-sensitive manner.

HuR Plays an Essential Role in piRNA-Induced, ARE-Dependent Target Activation

HuR has been known to be essential for spermatogenesis in mice (Nguyen-Chi et al., 2011). A previous study reported that HuR, a canonical ARE-binding protein, is associated with the traffic of ARE-containing mRNAs from the chromatoid body, a germ granule in round spermatids that has been suggested as a center for mRNA storage (Meikar et al., 2011), to polysomes (Nguyen-Chi et al., 2009). These prior observations thus point to a positive role of HuR in regulating a switch from mRNA storage to translation during spermiogenesis.

To test the hypothesis that HuR might be involved in piRNA-mediated translation activation, we first performed RIP assay on the series of *Grk4* 3′ UTR reporters and found that the ARE inserted at 1,350 nt in the *Grk4* 3′ UTR reporter led to a more efficient HuR-binding compared to its insertion at other locations in the same reporter (Figure 4B, right), correlating HuR-binding to piRNA-dependent translation activation. We extended the analysis to all five validated piRNA target mRNAs in mouse testes, finding that *Plectin, Agfg1, Tbpl1, Cnot4*, and *Atg12* mRNAs were all substantially enriched in anti-HuR immunoprecipitant compared to IgG control (Figure 4C), indicative of a strong association of these mRNAs with HuR *in vivo*. We further found that *HuR* knockdown completely abolished the effect of piRNAs on activating their target reporters (Figure 4D), which again barely altered the reporter mRNA levels (Figure S3B). These results strongly suggested HuR in target activation by the piRNA system.

We next examined whether HuR associates with MIWI and eIF3f. By coIP, we found that either Flag-tagged MIWI or eIF3f was unable to pull down Myc-HuR in co-transfected 293T cells (Figure S3C). However, co-transfection of the *Plectin* reporter and piR_1029 enabled the interaction between HuR and the MIWI/eIF3f complex (Figure S3D), suggesting that piRNA:mRNA pairing may bridge the interaction between HuR and the MIWI/eIF3f complex. Unlike 293T cells, mouse testes contain active piRNAs, and indeed, we detected significant association of endogenous HuR with both MIWI and eIF3f in mouse testes (Figure S3E). We further performed proteomic analyses in this biologically relevant system and detected eIF3f and HuR in anti-MIWI immunoprecipitant and, conversely, MIWI in anti-HuR immunoprecipitant from mouse testes (Table S2). As expected from RNA-bridged association, we confirmed that the association between HuR and MIWI was RNase A sensitive (Figure S3E). Together, these data provide both biochemical and functional evidence for a vital role of HuR in translation activation of ARE-containing MIWI/piRNA targets.

Both MIWI and HuR Associate with Multiple Translation-Related Proteins in Mouse Testes

Interestingly, we also identified several translation-related proteins in both anti-MIWI and anti-HuR IPed complexes from mouse testes (Table S2), including translation initiation factor eIF4G3 and poly(A) tail-binding proteins (PABPs). To further dissect the functional complexes, we immunopurified MIWI- or HuR-containing complexes from polysome fractions prepared from mouse testes for proteomic analysis and again confirmed the presence of these translation initiation factors in both anti-MIWI and anti-HuR IPed complexes (Figure S3H). These results suggest that MIWI and HuR associate with the competent translation initiation machinery in mouse testes.

eIF4G is essential for the assembly of the eIF4F complex and initiation of cap-dependent translation (Merrick, 2015). Interestingly, among three eIF4G isoforms, eIF4G3 is essential for male fertility in mice (Sun et al., 2010). We noted that a recent report also identified eIF4G3 as a HuR-interacting protein in mouse testes to facilitate dramatic translational reprogramming in post-meiotic spermatids together with additional associated translation factors (i.e., eIF4A2, eIF4E, and PABPC1; Hu et al., 2018). These findings thus point to a role of eIF4G3 in activating mRNA translation in post-meiotic spermatids. We confirmed the interaction of HuR with eIF4G3 by coIP in both mouse testes (Figure S3F) and co-transfected 293T cells (Figure S3G) and showed that their interaction was insensitive to RNase A treatment. These results thus suggest eIF4G3 as a component of the MIWI/piRNA/eIF3f/HuR super-complex in mouse testes.

PABP facilitates translation initiation via its association with eIF4G (Imataka et al., 1998), which has also been reported to associate with MIWI in mouse testes (Kimura et al., 2009). Two cytoplasmic PABP proteins, PABPC1 and PABPC2, have been characterized in mouse male germ cells, where PABPC1 appears to associate with actively translating polysomes whereas PABPC2 likely functions in translation repression during spermatogenesis (Kimura et al., 2009). Interestingly, we found that HuR effectively promoted the association of MIWI with PABPC1 (Figure S3I). Collectively, these biochemical data suggest that HuR may orchestrate translation activation of ARE-containing target mRNAs through recruiting multiple translation activators, particularly eIF4G3 and PABPC1.

Requirement of Both MIWI and HuR for Translation Activation in Mouse Spermatids

We next focused on examining the effect of the piRNA system on translation activation during spermatogenesis. To this end, we isolated spermatocytes (SCs) and haploid spermatids (STs) from mouse testes (Figure S4A) and examined the expression of three validated piRNA-activated targets, i.e., *Plectin, Agfg1*, and *Tbpl1*, in SCs and STs. We found similar levels of their mRNAs in both cell populations (Figure 5A, left), but their proteins were only readily detectable in STs (right). These developmental expression profiles are thus fully in line with the possibility that these piRNA target genes are transcribed in SCs but translationally activated in spermatids.

To directly demonstrate these decoupled transcription and translation events, we performed sucrose gradient analysis to assess the translation activity of the three mRNAs during male germ cell development. Due to severe collapse of polysomes from highly purified SCs and STs (data not shown), we then compared the polysome profiles of testicular tissues at two developmental time points: 18 days postpartum (dpp), which contains SCs but lacks STs, versus 30-dpp, which contains both SCs and STs. In spermatid-containing 30-dpp testes, the levels of all three mRNAs (Figure S4B) and their cognate piRNAs (Figure S4C), as well as MIWI and HuR proteins (Figure S4D), were significantly elevated in the polysome fractions with a concomitant decrease in lighter RNP and 40S-80S fractions compared to 18-dpp testes. Importantly, all three mRNAs showed increased association with MIWI and HuR on polysomes in 30-dpp testes relative to 18-dpp testes from our RIP analysis (Figure S4E). These data support the functional roles of MIWI and HuR in translation activation of these piRNA targets in mouse spermatids.

To directly document the requirement of the piRNA system in target mRNA translation in mouse spermatids, we used high-titer short hairpin RNA (shRNA) lentivirus to knock down *Miwi, HuR*, or *eIF3f* in mouse spermatids through testis transduction on 3- to 4-week-young mice. We found little toxicity with control pSilencer:GFP or *shMiwi* lentivirus on mouse testes. However, the shRNA lentivirus against *eIF3f* caused severe damage and necrosis in transduced testes, and that *shHuR* lentivirus gave rise to moderately damaged but still viable testes. These phenotypes likely result from eIF3f or HuR depletion-induced destruction of testicular structures, given that both eIF3f and HuR, unlike MIWI, are also constitutively expressed in testicular somatic cells. In any case, we performed immunostaining on the remaining GFP^+ spermatids and found that GFP^+ spermatids from both *shMiwi*:GFP and *shHuR*:GFP-transduced mice, but not pSilencer:GFP controls, showed a marked reduction of Plectin, Agfg1, and Tbpl1 proteins compared to GFP^- cells (Figures 5B, 5C, S4F, and S4G). We conclude from these data that both MIWI and HuR are required for translation activation of piRNA targets in mouse spermatids.

Blocking the MIWI-eIF3f Interaction Inhibits *Plectin* Expression in Mouse Spermatids

To begin to determine whether MIWI-binding to eIF3f is required for translation activation of piRNA targets in mouse spermatids, we mapped the domain(s) in MIWI responsible for eIF3f-binding by testing a series of MIWI truncation mutants (Figure S5A) for coIP with full-length eIF3f. We found that a 150-aa (amino acid) MIWI N-terminal peptide (MIWI-N2) efficiently interacted with eIF3f and deletion of 10 aa at position 111–120 (MIWI-$N2^{\Delta 111-120}$) abolished its binding with eIF3f (Figure S5B). Importantly, MIWI-N2, but not MIWI-$N2^{\Delta 111-120}$, effectively impaired the binding of full-length MIWI to eIF3f (Figure S5C). We further found that MIWI-N2, but not MIWI-$N2^{\Delta 111-120}$, significantly attenuated the effect of piR_1029 on the *Plectin* reporter (Figure S5D). These results indicate that MIWI-N2 is able to compete with full-length MIWI for binding to eIF3f.

The identification of such an interfering peptide afforded us a critical tool to test the functional requirement of the MIWI-eIF3f interaction for piRNA target expression in mouse spermatids. We therefore cloned Flag-tagged MIWI-N2 or MIWI-$N2^{\Delta 111-120}$ into pLVX-IRES-tdTomato lentiviral vector (Figure S5E) and expressed them in mouse spermatids through testis transduction on 3- to 4-week-young mice. Although this experiment could only yield a small number of $tdTomato^+$ spermatids, we managed to examine the effect of wild-type and mutant peptides on the expression of *Plectin*, a representative target, in $tdTomato^+$ spermatids by immunostaining. We found that transduction of the MIWI-N peptide, but not MIWI-$N2^{\Delta 111-120}$, led to an average of ~40% reduction of Plectin protein in mouse spermatids compared to untransduced cells (Figures 5D, S5F, and S5G). These results provide critical evidence for the functional requirement of the MIWI-eIF3f interaction for translation activation of piRNA targets in mouse spermatids.

Stage-Specific Association of MIWI with eIF3f/HuR during Spermatogenesis

Having established the functional requirement of MIWI and HuR proteins and the MIWI-eIF3f interaction for translation activation of piRNA targets in mouse spermatids, we next investigated how piRNA target mRNAs are selectively activated in a defined developmental window. To address this, we examined the assembly of the MIWI/eIF3f/HuR complex using

isolated mouse male germ cells (Figure S6, left). By double immunostaining of MIWI and eIF3f, we found that MIWI was largely separated from eIF3f in SCs, but the MIWI-containing granules came to partially colocalize with or in close proximity to eIF3f-containing granules in round spermatids (RSs), and finally, MIWI and eIF3f were separated from each other again in elongating spermatids (ESs; Figure S6, right). This indicates that the association of MIWI with eIF3f is temporally regulated during spermatogenesis.

To further corroborate this, we performed coIP experiments on three isolated cell populations, again confirming that MIWI was inefficient in association with either eIF3f or HuR in enriched SCs but showing significant interactions with both in enriched RSs, which were greatly attenuated in enriched ESs/Eds (elongating spermatids [ESs]/elongated spermatids [Eds]) (Figure 5E). In contrast, we found that MIWI was switched to interact with the deadenylase CAF1 in ES/Ed (Figure 5E), which is consistent with our previous observation for the assembly of the pi-RISC in late spermatids (Gou et al., 2014). This indicates that MIWI is switched from the translation-enhancing complex to the RNA decay complex during the progression of spermiogenesis. In fact, we further noted that both eIF3f and HuR proteins were sharply reduced in abundance in ES/Ed, while the levels of CAF1 protein were relatively consistent in all stages of spermatids. Collectively, our results indicate that the association of MIWI with eIF3f/HuR or CAF1 is temporally regulated during spermatogenesis and that the MIWI-containing translation activation complex is mainly assembled in round spermatids.

Global Evidence for a Large MIWI-Activated Translation Program in Mouse Spermatids

To generalize the findings based on a few piRNA targets characterized above, we next assessed how many genes might be subjected to activation by the piRNA system in mouse spermatids by performing ribosome profiling in parallel with RNA sequencing (RNA-seq). Because spermatogenesis is arrested at step 4 spermatids (corresponding to 24-dpp; Deng and Lin, 2002), we chose to compare between wild-type and *Miwi* null testes at this developmental stage. Having first shown typical 3-nt periodicity of ribosome protected fragments (RPFs) and established the reproducibility of our libraries (Figures S7A and S7B), we identified 3,959 mRNAs that showed significantly reduced translational efficiency based on RNA-seq-normalized RPFs in *Miwi* null testes relative to wild-type control (Figure 6A; Table S3). Gene Ontology (GO) analysis showed that many direct targets are involved in spermatogenesis, spermatid development including acrosome and flagellum formation, and sperm motility (Figure S7C). We noted that 3 out of the 5 validated piRNA targets (i.e., *Agfg1, Tbpl1*, and *Cnot4*) were identified with significantly reduced translational efficiency in *Miwi* null testes and the translational efficiency of *Atg12* appeared to be also reduced, though without sufficient statistical significance (Figure 6A; Table S3). However, few RPFs on the Plectin transcript were detected in either 24-dpp *Miwi* null or wild-type testes, suggesting little translation in spermatids prior to step 4, consistent with a previous report showing that Plectin protein began to be detectable at steps 8–9 spermatids (Johnson et al., 2004). These data suggest that MIWI may be directly or indirectly involved in regulating the translation of a large group of mRNAs in mouse testes.

We next sorted out MIWI and HuR co-bound piRNA targets for further comparative analysis. Using our previous MIWI CLIP-seq data in mouse spermatids (Gou et al., 2014; Zhang et al., 2015) and reported HuR-binding motifs (Lebedeva et al., 2011), we categorized mRNA transcripts in mouse spermatids into three groups: (1) non-targets (no MIWI CLIP reads), (2) MIWI targets (MIWI CLIP peaks in 3′ UTRs), and (3) MIWI/HuR co-targets (containing both MIWI and HuR-binding sites in 3′ UTRs). Indeed, relative to non-targets, we observed significantly decreased translational efficiency for MIWI targets and more pronounced decrease for MIWI/HuR co-targets in *Miwi* null testes compared to wild-type control ($p < 0.001$, Mann-Whitney U test; Figure 6B). Cross analysis revealed that 601 out of the 1,501 MIWI/HuR co-targets showed significantly reduced translational efficiency in *Miwi* null testes (Figure 6C), implicating this subset of genes as direct targets. These results suggest that MIWI may promote translation of its target genes in testes via multiple mechanisms, one of which is through co-binding with HuR to achieve robust translation activation.

To further determine the role of the piRNA system in translation activation during spermiogenesis, we examined the global effect of MIWI or HuR knockdown on protein expression in mouse spermatids. To engineer MIWI or HuR depletion in round spermatids, we carried out testis transduction on young mice at 3–4 weeks of age, which allowed us to obtain ~10^4–10^5 GFP^+ spermatids from 40 *shHuR*:GFP or *shMiwi*:GFP-transduced testes by unit gravity sedimentation coupled with fluorescence-activated cell sorting (FACS) procedures (Figure 6D). Western blotting verified a marked reduction of Plectin, Agfg1, and Tbpl1 proteins in *shMiwi*:GFP-transduced spermatids (Figure 6E), with few changes in their mRNA levels as quantified by qRT-PCR (Figure 6F). Using ~1×10^4 GFP^+ spermatids, we performed protein profiling on a sensitive nanoLC-MS/MS (liquid chromatography-tandem mass specrometry) instrument and detected ~300–500 proteins in spermatids transduced with control pSilencer:GFP, *shMiwi*:GFP, or *shHuR*:GFP, respectively. We noted that Plectin showed a ~3- to 6-fold reduction in MIWI- or HuR-depleted spermatids relative to controls (Table S4). Importantly, we found 123 and 132 proteins that were significantly reduced (>2-fold) in *shMiwi*:GFP- or *shHuR*:GFP-transduced cells, respectively (Figure 6G; Table S4). Cross analysis revealed that 71 proteins were shared between MIWI- and HuR-regulated proteins (Figure 6G), among which 37 genes contain MIWI and HuR-binding sites in their 3′ UTRs. These results together strongly support that MIWI and HuR may act in the same pathway to activate the translation of a subset of mRNAs in mouse spermatids.

MIWI-Activated Genes Critical for Acrosome Formation

Finally, we wished to provide the biological significance for MIWI/piRNA-induced target activation during spermatid development. To this end, we constructed a pLKO.1-shRNA-Cyto IV-fused EGFP lentiviral vector that contains a mitochondrial targeting signal (Cyto IV) fused to EGFP (Cyto IV-EGFP; Figure 7A, top), thus allowing us to track the progression of sperm maturation from transduced spermatids. We detected GFP^+ sperm in the epididymides of *shMiwi*-Cyto IV-EGFP-transduced mice, but not in *shHuR*-Cyto IV-EGFP or *sheIF3f*-Cyto IV-EGFP-transduced animals, indicating that both HuR and eIF3f have broader roles than MIWI in testes. Importantly, MIWI knockdown clearly impaired sperm maturation, because the counts of GFP^+ sperm in *shMiwi*-Cyto IV-EGFP-transduced

mice were dramatically reduced relative to the *shRNA*-Cyto IV-EGFP-transduced controls, supporting a functional requirement of MIWI for spermatozoa formation.

Given that *Agfg1* and *Tbpl1* have been shown to be essential for acrosome formation during spermatid development (Kang-Decker et al., 2001; Zhang et al., 2001), we inspected acrosomes in the sperm progressed from *shMiwi*-Cyto IV-EGFP-transduced spermatids by Peanut agglutinin (PNA) staining. Indeed, we observed severe defects at acrosomes in the *shMiwi*-Cyto IV-EGFP-transduced sperm, but not in the *shRNA*-Cyto IV-EGFP-transduced control (Figure 7B, top). These results demonstrated a functional requirement of MIWI for acrosome formation during spermiogenesis.

To further substantiate the functional role of MIWI/piRNA-induced target activation in acrosome formation, we asked whether the defective acrosome formation in *shMiwi*-Cyto IV-EGFP-transduced spermatids could be rescued by restoring Agfg1 or Tbpl1 protein in these cells. To this end, we constructed the pGK-driven Cyto IV-EGFP-IRES-Agfg1 or Tbpl1 into the pLKO.1-*shMiwi* lentiviral vector, in which *shMiwi* was co-expressed with the expression unit of Agfg1 or Tbpl1. We found little improvement of acrosomes in GFP^+ sperm from either *shMiwi*-Agfg1 or *shMiwi*-Tbpl1-transduced mice (data not shown), suggesting that single restoration of either Agfg1 or Tbpl1 protein in MIWI-depleted spermatids was not enough to rescue acrosomes in resulting sperm. We thus attempted to insert the pGK-driven Cyto IV-EGFP-IRES-Agfg1-IRES-Tbpl1 into the pLKO.1-*shMiwi* vector (Figure 7A, bottom) to co-express *shMiwi* with Agfg1 and Tbpl1 proteins. Immunostaining of enriched spermatids showed a dramatic reduction of Agfg1 and Tbpl1 proteins in *shMiwi*-Cyto IV-EGFP-transduced cells relative to untransduced GFP^- controls (Figure 7C, left) and successful restoration of both Agfg1 and Tbpl1 proteins in *shMiwi*-Agfg1/Tbpl1 vector-transduced spermatids (right). Remarkably, acrosomes were significantly recovered in >50% of GFP^+ sperm from *shMiwi*-Agfg1/Tbpl1-transduced mice (Figure 7D). These results unequivocally demonstrated that restoration of Agfg1 and Tbpl1 expression is able to significantly rescue defective acrosome formation in MIWI-depleted spermatids. Together, these results demonstrated that translationally activated *Agfg1* and *Tbpl1* by the newly elucidated function of the piRNA system plays a central role in acrosome formation during spermiogenesis.

DISCUSSION

An Unprecedented Function of the piRNA Machinery in Translational Control

Post-transcriptional gene regulation plays a vital role in postmeiotic male germ cell development in mammals. Although previous studies have revealed specific mechanisms for translational control of several spermiogenic mRNAs (Kwon and Hecht, 1991, 1993; Zhong et al., 1999, 2001; Tsai-Morris et al., 2012; Kleene, 2013; Nguyen-Chi and Morello, 2011), how a large variety of repressed mRNAs are activated during spermiogenesis has remained an open question. We now provide evidence that the MIWI/piRNA system plays a key role in translation activation in mouse spermatids, thus uncovering a previously unknown function of the piRNA machinery in male germ cell development.

Our findings provide mechanistic insights into the reported association of mouse PIWI proteins with the translation machinery (Grivna et al., 2006; Unhavaithaya et al., 2009) and a putative role of MIWI in stabilizing certain spermiogenic mRNA in mouse testes (Vourekas et al., 2012). Interestingly, the *Drosophila* PIWI protein Aubergine was also reported to interact with several translation initiation factors to promote translation of self-renewal and differentiation factors in germline stem cells (Ma et al., 2017), and the same protein was suggested to help stabilize certain mRNAs in a piRNA-dependent manner (Dufourt et al., 2017). These observations suggest that piRNA-activated translation may be a conserved mechanism in animals.

Stage-Specific Recruitment of Translation Initiation Factors to MIWI/piRNA Targets

As schemed in Figure 7E, piRNA-programmed translation activation requires specific recruitment of eIF3f by MIWI. However, this alone seems to be insufficient to activate translation, which also depends on the presence of an ARE adjacent to a piRNA target site in 3′ UTR. Such AREs help recruit the RNA-binding protein HuR, which in turn attracts eIF4G3, a specific eIF4G isoform known to be required for male germ cell development (Hu et al., 2018). Interestingly, while the interaction between MIWI and eIF3f and the interaction between HuR and eIF4G3 are both independent of RNA, the formation of the MIWI/eIF3/HuR/eIF4G3 super-complex is RNA mediated. Therefore, although eIF3 has been reported to be able to recruit eIF4G but without specificity for different eIF4G isoforms in other cellular systems (Gingras et al., 1999), our data indicate that eIF4G3 might be recruited and then stabilized by both MIWI/eIF3 and HuR in a synergistic fashion.

Importantly, such a super-complex is formed specifically in round spermatids based on our coIP and co-colocalization data. This stage-specific complex assembly likely accounts for the switch of target mRNAs from the stored to the activated state. However, all of these factors appear to be constitutively expressed in multiple developmental stages from SCs to round spermatids to elongating spermatids with detectable decline only in later elongated spermatids. We currently do not know how the super-complex is assembled in such a stage-specific manner, which may involve a stage-specific factor(s) and/or post-translational modifications of an existing factor(s) to be investigated in future studies.

The MIWI/piRNA System Drives a Large Translation Activation Program in Testes

Our current study began with pursuing an unexpected activation of a few MIWI/piRNA targets. However, given the enormous repertoire of the piRNA targeting capacity and the prevalent distribution of HuR-binding sites in the 3′ UTRs of numerous mRNAs (Lebedeva et al., 2011), the initial characterized targets appear to be the tip of the iceberg. Indeed, by ribosome profiling using *Miwi* null testes, we identified a group of ~600 mRNAs as direct piRNA targets for such regulation in mouse spermatids, and our nanoLC-MS/MS analysis further confirmed a number of targets at the protein levels.

Importantly, we showed that this newly elucidated function of piRNA system is critical for acrosome formation during spermiogenesis. Moreover, besides abnormal acrosomes, we found several other defects in the *shMiwi*:Cyto IV-EGFP-transduced sperm, including abnormal morphology, curved back heads, etc. This implies the contribution of the MIWI/

piRNA machinery to multiple developmental events during spermiogenesis via controlling various target genes. It will be interesting to determine whether and how the piRNA system plays such seemingly broad roles in facilitating the transformation of spermatids into spermatozoa.

A Dual Role of the MIWI/piRNA Machinery during Spermiogenesis

Our current findings extend in the function of the Piwi/piRNA machinery in regulating coding genes in animal germ cells. Previous studies from us and others demonstrate the function of piRNAs in inducing mRNA decay by using a miRNA/siRNA-like mechanism (Gou et al., 2014; Zhang et al., 2015; Goh et al., 2015; Watanabe et al., 2015; Vourekas et al., 2016; Shen et al., 2018; Zhang et al., 2018). Thus, the MIWI/piRNA machinery appears to have a dual function in regulating the fate of target mRNAs in mouse spermatids. In earlier stages of spermatids, the machinery is responsible for activating translation through the formation of the MIWI/piRNA/eIF3f/HuR super-complex. This complex appears to be switched to the MIWI/piRNA/CAF1 super-complex in later stages of spermatids to trigger massive mRNA elimination to inactivate the vast cellular programs in preparation for spermatozoa production from spermatids.

In conclusion, our present findings reveal an important role for the piRNA system in translation activation of spermiogenic mRNAs and demonstrate the critical importance of such regulation in acrosome formation during spermatid development in mice. Together with the elucidated function of the piRNA system in mRNA decay, our findings highlight a multifaceted function of the piRNA system in a highly orchestrated developmental program in male germ cells.

STAR★METHODS

LEAD CONTACT AND MATERIALS AVAILABILITY

Further information and requests for resources and reagents should be directed to and will be fulfilled by the Lead Contact, Mo-Fang Liu (mfliu@sibcb.ac.cn). All unique/stable reagents generated in this study are available from the Lead Contact with a completed Materials Transfer Agreement.

EXPERIMENTAL MODEL AND SUBJECT DETAILS

Cell Culture and Transfections—Two cell lines were used in this study: Female Human Embryonic Kidney 293T (293T) and Male mouse spermatocyte-derived GC-2spd (ts) cells have been authenticated. Cells were cultured in DMEM with 10% FBS. Transfections were performed with Lipofectamine 2000 (Invitrogen) for 293T cells or Lipofectamine 3000 (Invitrogen) for GC-2spd (ts) cells according to the manufacturer's instructions. All DNA plasmids were cleared of endotoxin.

Mice—Male C57BL6 mice at 18-dpp, 30-dpp, 3-4 weeks (young) or 8 weeks (adult) of age were used in this study. *Miwi* knockout mice (Deng and Lin, 2002) were purchased from Mutant Mouse Resource Research Centers. Male *Miwi* null and control mice at 24-dpp of age were used in this study. All mice were housed in the SIBCB animal facility under SPF

conditions in accordance with institutional guidelines and ethical regulations and fed with regular chow and water by the facility staff. All experimental animal procedures were approved by the Institutional Animal Care and Research Advisory Committee at SIBCB, CAS.

METHOD DETAILS

Plasmids and RNA oligonucleotides—For *Renilla* luciferase 3′ UTR reporters, the 3′ UTRs of mouse *Plectin* (~1.2 kb), *Agfg1* (~1.2 kb), *Tbpl1* (~1.9 kb), *Cnot4* (~1.5 kb) and *Atg12* (~2 kb) were cloned downstream of the *Renilla* luciferase gene in pRL-TK (Promega), respectively. To generate the mutant 3′ UTR reporters, seven or eight nucleotides in each 3′ UTR complementary to the 5′ portion of cognate piRNA were deleted using KOD-Plus-mutagenesis kit (Figure 1A). p3xFlag-MIWI, p3xFlag-HIWI, and Flag-Y345/346A HIWI were constructed as we recently reported. p3xFlag-eIF3f, p3xFlag-eIF4G3, pCMV-Myc-eIF3f, pCMV-Myc-HuR, pCMV-Myc-PABPC1 and pCMV-Myc-PABPC2 were constructed through insertion of the cDNAs without the 3′ UTRs of mouse *eIF3f* (NM_025344.2), *eIF4g3* (NM_172703.3), *HuR* (NM_010485.3), *Pabpc1* (NM_008774.3) and *Pabpc2* (NM_011033.2) into p3 × Flag-CMV-10 (Sigma) and pCMV-Myc (Clontech), respectively. p3xFlag-MIWI was used to generate MIWI truncation mutants (Figure S5A) with KOD-Plus-mutagenesis kit. To construct GST-fused eIF3f for bacterial expression, mouse *eIF3f* cDNA was inserted into pGEX-KG (ATCC). The lentiviral shRNA vectors targeting mouse *Miwi* and *HuR* were constructed using pSilencer-H1-LV as we recently described (Gou et al., 2014; Zhao et al., 2013). The lentiviral vectors pLKO.1-shRNA-CytoIV-fused EGFP were generated using pLKO.1 (Addgene), and inserted with pGK-driven CytoIV-EGFP [a mitochondrial targeting signal (Cyto) fused EGFP] or pGK-driven CytoIV-EGFP-IRES-Agfg1-IRES-Tbpl1 (Figure 7A). The lentiviral vectors pLVX-Flag-MIWI-N2-IRES-tdTomato and pLVX-Flag-MIWI-N2$^{\Delta 111–120}$-IRES-tdTomato were generated using pLVX-IRES-tdTomato (Clontech; Figure S5E). All constructs were confirmed by DNA sequencing. All RNA oligonucleotides, including piRNAs and siRNAs, were synthesized by Ribobio or Biotend (China), and their sequences were listed in the Key Resource Table and Tables S5 and S6. All chemically synthetic piRNAs are containing phosphate at the 5′ ends and 2′-O-methylation at the 3′ ends.

Luciferase reporter assay—Luciferase reporter assays were carried out as we described previously (Gou et al., 2014). In brief, GC-2spd (ts) cells were co-transfected in 24-well plates with chemically synthetic piRNAs, *Renilla* luciferase 3′ UTR reporters, or/and siRNAs or protein expression vectors. The firefly luciferase plasmid pGL3 was used as an internal control. Dual luciferase reporter assays were performed 24 h after transfection using Dual-Glo Luciferase Assay Systems (Promega).

Immunoprecipitation, immunoblotting, and immunofluorescent microscopy (IF)—For immunoprecipitation, cells or testicular tissue were homogenized in iced lysis buffer [50 mM Tris-HCl (pH 7.4), 1% Triton X-100, 150 mM NaCl, 5 mM EDTA, and protease inhibitor cocktail]. Cell or tissue extracts were incubated with antibody-coupled Protein A beads or Protein G beads (Sigma) according to the manufacturer's Instructions. For immunoblotting, IP pellets or cell/tissue extracts were diluted in SDS loading buffer and

subjected to standard SDS-PAGE and western blotting procedures. Western blotting images were captured by Tanon-5200 Chemiluminescent Imaging System (Tanon). For IF, enriched spermatids or sperm from the cauda epididymis were fixed with 4% paraformaldehyde, permeabilized with 0.5% Triton X-100 in PBS, and incubated with primary antibodies and Alexa Fluor 488 or Cy3-conjugated secondary antibodies or with PNA conjugated with Alexa Fluor 594 (Molecular probes). Nuclei were counterstained with DAPI (Vector Laboratories). Images were captured using a Nikon DS-Ri2 microscope, and immunofluorescent densities were quantified using imageJ software.

RNA isolation, qRT-PCR, and RIP assays—The assays were performed as we described recently (Zhao et al., 2013; Gou et al., 2014). In brief, total RNAs in cells or tissues were extracted with RNAiso Plus (Takara) according to the manufacturer's protocol. Reverse transcription and qRT-PCR were performed using PrimeScript RT and SYBR Green kits (Takara) on a QuantStudio 3 system (Applied Biosystems) according to the manufactures' protocols. For RIP assays, cells or tissues were homogenized in lysis buffer [100 mM KCl, 5 mM MgCl2,10 mM HEPES, 0.5% NP-40 containing 10 U/mL RNase inhibitor (Takara) and a protease inhibitor cocktail (Roche)] and extracts were incubated with IgG, anti-MIWI, or anti-HuR antibody-coupled Protein A/G for 4 h at 4°C. RIP analyses of sucrose gradient fractions were performed as described previously (Vasudevan and Steitz, 2007). In brief, the indicated fractions derived from sucrose gradients were incubated with IgG, anti-MIWI, or anti-HuR antibody-coupled Protein A/G for 4 h at 4°C. After stringently washing the beads with washing buffer [50 mM Tris-HCl (pH 7.4), 0.1% Triton X-100, 500 mM NaCl, 5 mM EDTA, protease inhibitor cocktail and RNase inhibitor], total RNAs were extracted with TRIzol and subjected to qRT-PCR assays. The primer sequences for qRT-PCR were provided in the Key Resource Table and Table S5. The results were analyzed and shown as relative piRNA or mRNA levels of the CT (cycle threshold) values, which were then converted as fold change.

GST pull-down—GST pull-down was performed as we previously described (Zhao et al., 2013). In brief, MIWI protein was prepared in the presence of S^{35}-labeled methionine using the transcription and translation (TNT) system (Promega). GST-fusion eIF3f was expressed in *E.coli* BL21, purified and immobilized on glutathione agarose beads. The beads were blocked with PBS containing 0.1% NP-40 (v/v), 5 mM EDTA, 5 mM EGTA, 20 mM leupeptin, 25 mg/mL ALLN, 5 mg/mL pepstatin A, and 2 mg/mL aprotinin plus 5% nonfat milk, and incubated with [^{35}S]Met-MIWI for 2 h at 4°C. After five time stringently washing, the bound proteins were dissolved in SDS sample buffer, separated by SDS-PAGE, and subjected to autoradiography.

Sucrose gradient analysis—Sucrose gradient analysis was performed as described previously (Hawthorne et al., 2006). In brief, cells or testicular tissues from 18-dpp or 30-dpp mice were homogenized in extraction buffer (PEB) [100 mM NaCl, 50 mM Tris·HCl, pH 7.5, 5 mM $MgCl_2$,1% Triton X-100,100 μg/mL cycloheximide (CHX)], and were subjected to centrifugation at 13,000 g for 2 min to remove nuclear pellets. The extracts were then layered over 10%–60% sucrose gradients and centrifuged at 39,000 rpm on the SW 41 rotor for 2 h at 4°C. Twelve fractions were collected, and each fraction was subjected

to western blotting and RT-qPCR analyses of indicated proteins and RNAs, respectively. For Sucrose gradient analysis of GC-2spd (ts) cells, 24 h post-transfection, cells were pre-incubated with cycloheximide (Sigma; 100 μg/mL for 15 min) and then subjected to preparation of cytoplasmic lysates. The lysates were fractionated by ultra-centrifugation through 10%–60% sucrose gradients and then separated into ~1,200 fractions using a Piston Gradient Fractionator (Biocomp, Fredericton, Canada).

Isolation of mouse SCs, STs, and GFP$^+$ spermatids—Isolation of SCs and STs from mouse testes was performed as we recently described (Zhao et al., 2013; Gou et al., 2014). In brief, total spermatogenic cells were extracted from the seminiferous tubules of indicated male mice, and SCs and STs were separated through the unit gravity sedimentation procedure. Then round spermatids and later stages of spermatids (consisting of ESs and Eds) were separated from haploid spermatid fractions through FACS. GFP$^+$ spermatids were sorted through FACS from haploid spermatid fractions obtained from transduced testes. The isolated spermatogenic cells were all confirmed by their distinct nuclear morphology (DAPI staining of nuclei).

Lentivirus packaging and testis transduction—Lentivirus packaging and testis transduction were performed as we recently described (Zhao et al., 2013). In brief, the lentiviral vectors were packaged into pseudovirus with their cognate packaging plasmids following standard procedures. High-titer lentivirus (> 10^8 transduction units/mL) was prepared by ultra-centrifugation. About 10 μL of high-titer lentivirus were injected into seminiferous tubule through the efferent duct via a sharp glass capillary with a tip diameter of 50 μm. The testes were harvested a week post-transduction of shRNA expression vectors for examining transduced spermatids, while epididymides were harvested two weeks post-transduction for examining sperm progressed from transduced spermatids.

Proteomics and protein profiling analyses—Proteomics analysis of anti-MIWI or anti-HuR IPed complexes from mouse testicular lysates or polysome fractions from mouse testicular lysates prepared by 10%–60% sucrose gradients were analyzed by gel-free LC-MS/MS (Thermo Scientific) according to the manufacture's protocol. In brief, Cells were lysed in a buffer (8 M urea, 4% CHAPS, 40 mM Tris-HCl, 65 mM DTT, 1 mM PMSF, 1 mM EDTA, 0.5 mM EGTA). After shaking for 1 min, the cells were subjected to ultrasonic treatment for 10 min (at an 80 W sonic power, working for 3 s and stop for 3 s). Lysates were then clarified at 20,000 g for 15 min. Total protein concentrations were determined using the bicinchoninic acid (BCA) protein assay kit. The proteins were alkylated with 300 mM iodoacetamide in the dark for 40 min, and digested with trypsin (1:25, Promega) overnight at 37°C via the FASP protocol with spin ultrafiltration units of nominal molecular weight cutoff 10,000 (Wiśniewski et al., 2009). Protein profiling of GFP$^+$ spermatids (~1×10^4) were performed on the nanoLC-MS/MS system. The nanoLC-MS/MS analysis was performed using an EASY-nL 1200 system coupled online to a QExactive plus mass spectrometer (Thermo Scientific, Bremen, Germany). Briefly, aliquots containing 1-2 μg of peptides were injected and separated on a reversed-phase column (15cm μ 50 μm, 2 μm, Dionex, Thermofisher) using a 2 h acetonitrile gradient in 0.1% formic acid at a flow rate of 300 nL/min.

The MaxQuant (version 1.5.3.30) software was used to analyze the MS/MS raw data. For the database searching parameters, the precursor mass tolerance was set to 15 ppm. Trypsin/P was set as the protease, accounting for in-source fragmentation of lysine or arginine residues followed by proline. Two missed cleavages were allowed. All data were searching against with the UniProt Mouse database (sequences) including oxidation (+15.9949 Daltons) of methionine as dynamic modifications, and carbamidomethylation (+57.0215 Daltons) of cysteine as static modifications.

Ribosome profiling—Ribosome profiling was performed with a procedure modified from the method described previously (Ingolia et al., 2012). In brief, mouse testicular lysates were generated using 24-dpp *Miwi*$^{-/-}$ testes or wild-type controls in the presence of 100 μg/mL cycloheximide. The DNase-treated lysates were clarified by centrifugation and subjected to RNA extraction & sequencing or ribosome profiling analyses. For ribosome profiling, the lysates were further layered over 10%–60% sucrose gradients to prepare polysome fractions. The obtained polysomes were treated with RNase I and then subjected to purification of ~30 nt ribosome protected fragments using a 15% TBE-Urea gel. The fragments were subjected to RNA sequencing analysis using the Illumina sequencing technology, and sequences were processed and analyzed in the same manner as CLIP-seq data below.

QUANTIFICATION AND STATISTICAL ANALYSIS

CLIP-seq analysis—For CLIP-seq analysis, the anti-MIWI CLIP-seq data in enriched mouse spermatids were obtained from the Gene Expression Omnibus: SRP043638 and GSE67683 (Gou et al., 2014; Zhang et al., 2015). For quality control, the reads of CLIP-seq were subjected to removal of adapter sequences by cutadapt program (Martin, 2011) under parameters “—max-n 3 –e 0.1”. For the samples from GSE67683, the first 4 nt was extracted as barcode, and only one read from the reads group with the same sequence and barcode was kept to remove potential PCR bias. The reads that can be mapped to mouse rRNA sequences were removed using bowtie program (Langmead et al., 2009). The reads longer than 15-nt were mapped to GRCm38.p4 genome sequences by bowtie2 under parameters “--no-unal --end-to-end -k 10 --al” (Langmead and Salzberg, 2012). Only the primary alignments were retained for analysis. To call MIWI peaks, the transcript was scanned using a 10-nt sliding window with 1-nt step. The window was called as positive if the mean coverage was larger than or equal to sample-specific threshold from 3 to 6 by library size, and overlapping positive windows were merged as peaks. The genes with peak at their 3′ UTR are considered as MIWI-CLIP target genes, among which the genes containing more than two HuR motifs (UUUUUUU, UUUAUUU, UUUGUUU, UAUUUAU, AUUUUUA, AUUUAUU, AAUUUUA, and AAUAUUU) in their 3′ UTR are considered as common target genes.

RNA-seq and Ribo-seq analyses—For RNA-seq and Ribo-seq analyses, the adaptor sequences were first removed from Illumina sequencing reads. For RNA-seq reads, the adapters were trimmed by cutadapt program (Martin, 2011) with parameters “-m 18 -e 0.15,” while for Ribo-seq reads, the adapters were trimmed, and the random barcodes were extracted and appended to read names by custom script. To remove potential rRNA contamination, the reads were mapped to rRNA sequences with bowtie program (Langmead

et al., 2009), and those not mapped were then mapped to the mouse genome with gene annotation (GRCm38.p4 and Gencode.vM20) by using STAR program (Dobin et al., 2013) in global mode. The primary and proper-paired alignments were extracted from mapping results by BAMTools (Barnett et al., 2011) for further downstream analysis. For Ribo-seq samples, only one fragment from those with the same genomic signature (chromosome, start, end, and gaps) and same barcode was kept. For fragments within range from 28 nt to 30 nt, the 13th base located at the 1st position of codons were treated as canonical ribosome-protected fragments (RPFs) for the translation efficiency analysis. The $FPKM_{cds}$ (FPKM of CDS region) of each transcript was calculated as C * 1e9 / (L * N), where C represents the count of fragments that overlap with CDS region; L is the length of CDS; and N represents the total fragment count of the library. $FPKM_{cds\_RPF}$ and $FPKM_{cds\_rna}$ for each transcript were calculated from Ribo-seq and matched RNA-seq data, respectively. The translation efficiency was calculated as $FPKM_{cds\_RPF}/FPKM_{cds\_rna}$, and only those transcripts with $FPKM_{cds\_rna} >= 1$ and $C_{cds} >= 50$ were used for downstream analysis.

Other analyses—Gene Ontology (GO) term analyses were performed by DAVID (https://david.ncifcrf.gov/summary.jsp).

Student's t test was performed to compare the differences between treated groups relative to their paired controls. All results were presented as the mean ± SD *P*-values are indicated in the text or figures above the two groups compared with a value < 0.05 (denoted by asterisks) considered significant (***p < 0.001, **p < 0.01).

DATA AND CODE AVAILABILITY

All data presented are available in the main text and supplementary materials. The accession number for Ribo-seq reported in this paper is GSE139399.

Supplementary Material

Refer to Web version on PubMed Central for supplementary material.

ACKNOWLEDGMENTS

We thank members of the M.-F.L. and Y.Z. labs and Dr. Hong Cheng from SIBCB, CAS, for helpful comments. We thank Drs. Jianhua Yang from Sun Yat-sen University; Hu Zhou and Hongwen Zhu from SIMM, CAS; Peng Zhang from the University of Texas MD Anderson Cancer Center; and Xiaorong Zhang and Yuanchao Xue from IBP, CAS, for experimental assistance. This work was supported by grants from the National Key R&D Program of China (2017YFA0504400), Chinese Academy of Sciences ("Strategic Priority Research Program" grant XDB19010203), National Natural Science Foundation of China (31830109, 31821004, 91940305, and 91640201), Shanghai Municipal Science and Technology Major Project (17JC1420100, 19JC1410200, and 2017SHZDZX01), and the Foundation of Key Laboratory of Gene Engineering of the Ministry of Education. P.D. was supported by the SA-SIBS Scholarship Program and China Postdoctoral Science Foundation (2016M600335). L.-T.G. and X.-D.F. were supported by the NIH (grants GM052872 and HG004659).

REFERENCES

Barnett DW, Garrison EK, Quinlan AR, Strömberg MP, and Marth GT (2011). BamTools: a C++ API and toolkit for analyzing and managing BAM files. Bioinformatics 27, 1691–1692. [PubMed: 21493652]

Deng W, and Lin H (2002). *miwi*, a murine homolog of piwi, encodes a cytoplasmic protein essential for spermatogenesis. Dev. Cell 2, 819–830. [PubMed: 12062093]

Dobin A, Davis CA, Schlesinger F, Drenkow J, Zaleski C, Jha S, Batut P, Chaisson M, and Gingeras TR (2013). STAR: ultrafast universal RNA-seq aligner. Bioinformatics 29, 15–21. [PubMed: 23104886]

Dufourt J, Bontonou G, Chartier A, Jahan C, Meunier AC, Pierson S, Harrison PF, Papin C, Beilharz TH, and Simonelig M (2017). piRNAs and Aubergine cooperate with Wispy poly(A) polymerase to stabilize mRNAs in the germ plasm. Nat. Commun 8, 1305. [PubMed: 29101389]

Gingras AC, Raught B, and Sonenberg N (1999). eIF4 initiation factors: effectors of mRNA recruitment to ribosomes and regulators of translation. Annu. Rev. Biochem 68, 913–963. [PubMed: 10872469]

Goh WS, Falciatori I, Tam OH, Burgess R, Meikar O, Kotaja N, Hammell M, and Hannon GJ (2015). piRNA-directed cleavage of meiotic transcripts regulates spermatogenesis. Genes Dev. 29, 1032–1044. [PubMed: 25995188]

Gou LT, Dai P, Yang JH, Xue Y, Hu YP, Zhou Y, Kang JY, Wang X, Li H, Hua MM, et al. (2014). Pachytene piRNAs instruct massive mRNA elimination during late spermiogenesis. Cell Res. 24, 680–700. [PubMed: 24787618]

Gou LT, Kang JY, Dai P, Wang X, Li F, Zhao S, Zhang M, Hua MM, Lu Y, Zhu Y, et al. (2017). Ubiquitination-Deficient Mutations in Human Piwi Cause Male Infertility by Impairing Histone-to-Protamine Exchange during Spermiogenesis. Cell 169, 1090–1104.e13. [PubMed: 28552346]

Grivna ST, Pyhtila B, and Lin H (2006). MIWI associates with translational machinery and PIWI-interacting RNAs (piRNAs) in regulating spermatogenesis. Proc. Natl. Acad. Sci. USA 103, 13415–13420. [PubMed: 16938833]

Hasuwa H, Ishino K, and Siomi H (2018). Human PIWI (HIWI) is an azoospermia factor. Sci. China Life Sci 61, 348–350. [PubMed: 28801861]

Hawthorne SK, Busanelli RR, and Kleene KC (2006). The 5′ UTR and 3′ UTR of the sperm mitochondria-associated cysteine-rich protein mRNA regulate translation in spermatids by multiple mechanisms in transgenic mice. Dev. Biol 297, 118–126. [PubMed: 16759650]

Hofmann MC, Abramian D, and Millán JL (1995). A haploid and a diploid cell coexist in an in vitro immortalized spermatogenic cell line. Dev. Genet 16, 119–127. [PubMed: 7736662]

Hu J, Sun F, and Handel MA (2018). Nuclear localization of EIF4G3 suggests a role for the XY body in translational regulation during spermatogenesis in mice. Biol. Reprod 98, 102–114. [PubMed: 29161344]

Imataka H, Gradi A, and Sonenberg N (1998). A newly identified N-terminal amino acid sequence of human eIF4G binds poly(A)-binding protein and functions in poly(A)-dependent translation. EMBO J. 17, 7480–7489. [PubMed: 9857202]

Ingolia NT, Brar GA, Rouskin S, McGeachy AM, and Weissman JS (2012). The ribosome profiling strategy for monitoring translation in vivo by deep sequencing of ribosome-protected mRNA fragments. Nat. Protoc 7, 1534–1550. [PubMed: 22836135]

Iwasaki YW, Siomi MC, and Siomi H (2015). PIWI-Interacting RNA: Its Biogenesis and Functions. Annu. Rev. Biochem 84, 405–433. [PubMed: 25747396]

Johnson KJ, Zecevic A, and Kwon EJ (2004). Protocadherin alpha3 acts at sites distinct from classic cadherins in rat testis and sperm. Biol. Reprod 70, 303–312. [PubMed: 14522826]

Kang-Decker N, Mantchev GT, Juneja SC, McNiven MA, and van Deursen JM (2001). Lack of acrosome formation in Hrb-deficient mice. Science 294, 1531–1533. [PubMed: 11711676]

Kimura M, Ishida K, Kashiwabara S, and Baba T (2009). Characterization of two cytoplasmic poly(A)-binding proteins, PABPC1 and PABPC2, in mouse spermatogenic cells. Biol. Reprod 80, 545–554. [PubMed: 19020299]

Kleene KC (2013). Connecting cis-elements and trans-factors with mechanisms of developmental regulation of mRNA translation in meiotic and haploid mammalian spermatogenic cells. Reproduction 146, R1–R19. [PubMed: 23579190]

Kwon YK, and Hecht NB (1991). Cytoplasmic protein binding to highly conserved sequences in the 3′ untranslated region of mouse protamine 2 mRNA, a translationally regulated transcript of male germ cells. Proc. Natl. Acad. Sci. USA 88, 3584–3588. [PubMed: 2023906]

Kwon YK, and Hecht NB (1993). Binding of a phosphoprotein to the 3′ untranslated region of the mouse protamine 2 mRNA temporally represses its translation. Mol. Cell. Biol 13, 6547–6557. [PubMed: 8413253]

Langmead B, and Salzberg SL (2012). Fast gapped-read alignment with Bowtie 2. Nat. Methods 9, 357–359. [PubMed: 22388286]

Langmead B, Trapnell C, Pop M, and Salzberg SL (2009). Ultrafast and memory-efficient alignment of short DNA sequences to the human genome. Genome Biol. 10, R25. [PubMed: 19261174]

Lebedeva S, Jens M, Theil K, Schwanhäusser B, Selbach M, Landthaler M, and Rajewsky N (2011). Transcriptome-wide analysis of regulatory interactions of the RNA-binding protein HuR. Mol. Cell 43, 340–352. [PubMed: 21723171]

Ma X, Zhu X, Han Y, Story B, Do T, Song X, Wang S, Zhang Y, Blanchette M, Gogol M, et al. (2017). Aubergine Controls Germline Stem Cell Self-Renewal and Progeny Differentiation via Distinct Mechanisms. Dev. Cell 41, 157–169.e5. [PubMed: 28441530]

Marchione R, Leibovitch SA, and Lenormand JL (2013). The translational factor eIF3f: the ambivalent eIF3 subunit. Cell. Mol. Life Sci 70, 3603–3616. [PubMed: 23354061]

Martin M (2011). Cutadapt removes adapter sequences from high-throughput sequencing reads. EMBnet 17. 10.14806/ej.17.1.200.

Meikar O, Da Ros M, Korhonen H, and Kotaja N (2011). Chromatoid body and small RNAs in male germ cells. Reproduction 142, 195–209. [PubMed: 21652638]

Meistrich ML, and Hess RA (2013). Assessment of spermatogenesis through staging of seminiferous tubules. Methods Mol. Biol 927, 299–307. [PubMed: 22992924]

Merrick WC (2015). eIF4F: a retrospective. J. Biol. Chem 290, 24091–24099. [PubMed: 26324716]

Nguyen-Chi M, Auriol J, Jégou B, Kontoyiannis DL, Turner JM, de Rooij DG, and Morello D (2011). The RNA-binding protein ELAVL1/HuR is essential for mouse spermatogenesis, acting both at meiotic and postmeiotic stages. Mol. Biol. Cell 22, 2875–2885. [PubMed: 21737689]

Nguyen-Chi M, Chalmel F, Agius E, Vanzo N, Khabar KS, Jégou B, and Morello D (2009). Temporally regulated traffic of HuR and its associated ARE-containing mRNAs from the chromatoid body to polysomes during mouse spermatogenesis. PLoS ONE 4, e4900. [PubMed: 19333380]

Nguyen-Chi M, and Morello D (2011). RNA-binding proteins, RNA granules, and gametes: is unity strength? Reproduction 142, 803–817. [PubMed: 21976618]

Sassone-Corsi P (2002). Unique chromatin remodeling and transcriptional regulation in spermatogenesis. Science 296, 2176–2178. [PubMed: 12077401]

Shen EZ, Chen H, Ozturk AR, Tu S, Shirayama M, Tang W, Ding YH, Dai SY, Weng Z, and Mello CC (2018). Identification of piRNA Binding Sites Reveals the Argonaute Regulatory Landscape of the C. elegans Germline. Cell 172, 937–951.e18. [PubMed: 29456082]

Siomi MC, Sato K, Pezic D, and Aravin AA (2011). PIWI-interacting small RNAs: the vanguard of genome defence. Nat. Rev. Mol. Cell Biol 12, 246–258. [PubMed: 21427766]

Steger K (1999). Transcriptional and translational regulation of gene expression in haploid spermatids. Anat. Embryol. (Berl.) 199, 471–487. [PubMed: 10350128]

Sun F, Palmer K, and Handel MA (2010). Mutation of Eif4g3, encoding a eukaryotic translation initiation factor, causes male infertility and meiotic arrest of mouse spermatocytes. Development 137, 1699–1707. [PubMed: 20430745]

Tsai-Morris CH, Sato H, Gutti R, and Dufau ML (2012). Role of gonadotropin regulated testicular RNA helicase (GRTH/Ddx25) on polysomal associated mRNAs in mouse testis. PLoS ONE 7, e32470. [PubMed: 22479328]

Unhavaithaya Y, Hao Y, Beyret E, Yin H, Kuramochi-Miyagawa S, Nakano T, and Lin H (2009). MILI, a PIWI-interacting RNA-binding protein, is required for germ line stem cell self-renewal and appears to positively regulate translation. J. Biol. Chem 284, 6507–6519. [PubMed: 19114715]

Vasudevan S, and Steitz JA (2007). AU-rich-element-mediated upregulation of translation by FXR1 and Argonaute 2. Cell 128, 1105–1118. [PubMed: 17382880]

Vourekas A, Zheng Q, Alexiou P, Maragkakis M, Kirino Y, Gregory BD, and Mourelatos Z (2012). Mili and Miwi target RNA repertoire reveals piRNA biogenesis and function of Miwi in spermiogenesis. Nat. Struct. Mol. Biol 19, 773–781. [PubMed: 22842725]

Vourekas A, Alexiou P, Vrettos N, Maragkakis M, and Mourelatos Z (2016). Sequence-dependent but not sequence-specific piRNA adhesion traps mRNAs to the germ plasm. Nature 531, 390–394. [PubMed: 26950602]

Watanabe T, Cheng EC, Zhong M, and Lin H (2015). Retrotransposons and pseudogenes regulate mRNAs and lncRNAs via the piRNA pathway in the germline. Genome Res. 25, 368–380. [PubMed: 25480952]

Wiśniewski JR, Zougman A, Nagaraj N, and Mann M (2009). Universal sample preparation method for proteome analysis. Nat. Methods 6, 359–362. [PubMed: 19377485]

Yan W (2009). Male infertility caused by spermiogenic defects: lessons from gene knockouts. Mol. Cell. Endocrinol 306, 24–32. [PubMed: 19481682]

Zhang D, Penttila TL, Morris PL, Teichmann M, and Roeder RG (2001). Spermiogenesis deficiency in mice lacking the Trf2 gene. Science 292, 1153–1155. [PubMed: 11352070]

Zhang P, Kang JY, Gou LT, Wang J, Xue Y, Skogerboe G, Dai P, Huang DW, Chen R, Fu XD, et al. (2015). MIWI and piRNA-mediated cleavage of messenger RNAs in mouse testes. Cell Res. 25, 193–207. [PubMed: 25582079]

Zhang D, Tu S, Stubna M, Wu WS, Huang WC, Weng Z, and Lee HC (2018). The piRNA targeting rules and the resistance to piRNA silencing in endogenous genes. Science 359, 587–592. [PubMed: 29420292]

Zhao S, Gou LT, Zhang M, Zu LD, Hua MM, Hua Y, Shi HJ, Li Y, Li J, Li D, et al. (2013). piRNA-triggered MIWI ubiquitination and removal by APC/C in late spermatogenesis. Dev. Cell 24, 13–25. [PubMed: 23328397]

Zhong J, Peters AH, Lee K, and Braun RE (1999). A double-stranded RNA binding protein required for activation of repressed messages in mammalian germ cells. Nat. Genet 22, 171–174. [PubMed: 10369260]

Zhong J, Peters AH, Kafer K, and Braun RE (2001). A highly conserved sequence essential for translational repression of the protamine 1 messenger rna in murine spermatids. Biol. Reprod 64, 1784–1789. [PubMed: 11369609]

Highlights

- MIWI/piRNA activates mRNA translation via imperfect base-pairing interactions
- HuR and eIF3f are required for MIWI/piRNA-mediated target mRNA activation
- piRNA system controls the translation of a subset of mRNAs in mouse spermatids
- piRNA system plays a central role in acrosome formation during spermiogenesis

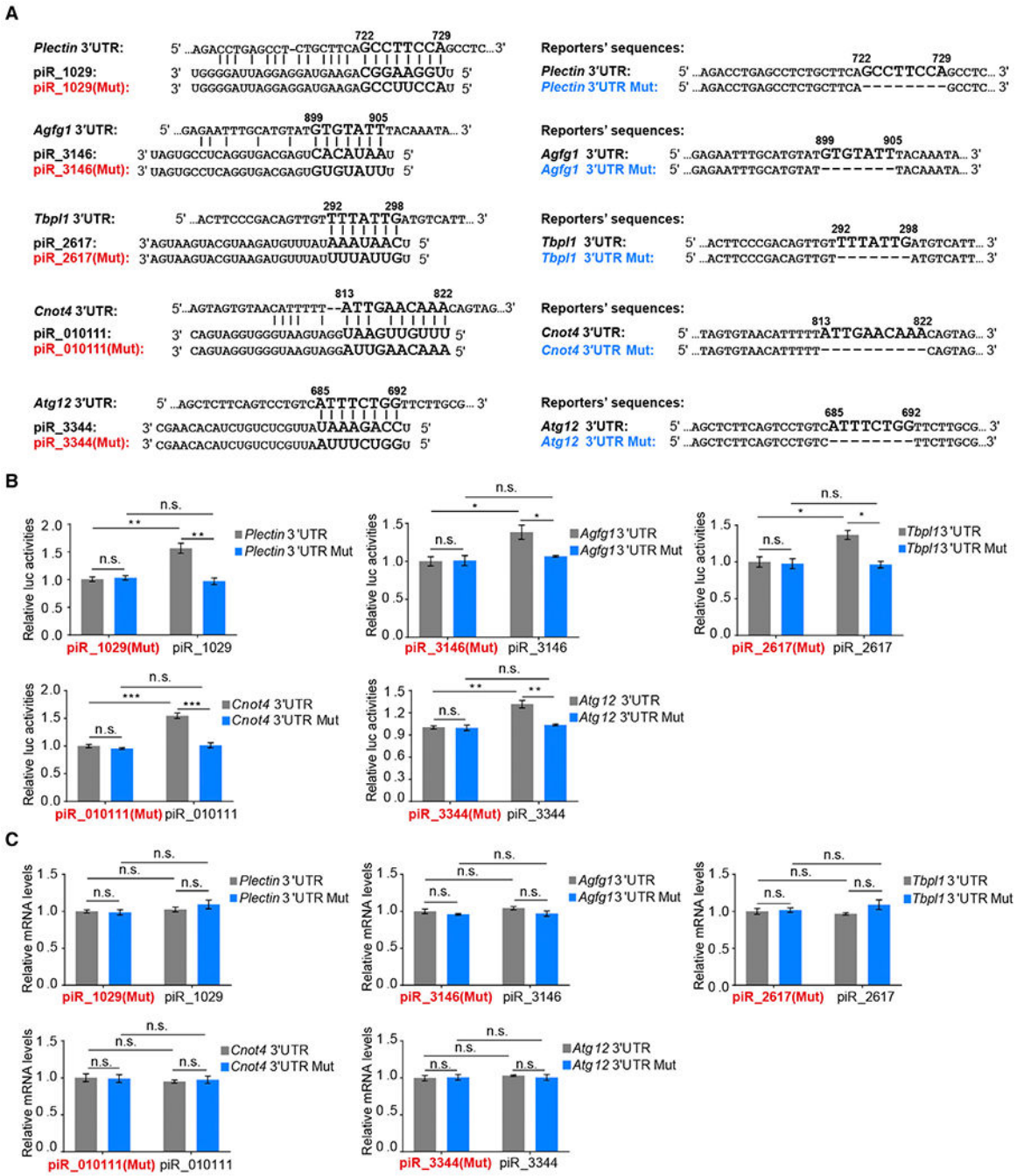

Figure 1. piRNAs Activate the Translation of Target mRNAs via Imperfectly Base Pairing with the 3′ UTRs

(A) Predicted piRNA regulatory elements at the 3′ UTRs of *Plectin, Agfg1, Tbpl1, Cnot4*, or *Atg12* and the synthetic piRNAs, mutated piRNAs, and wild-type and mutated 3′ UTR *Renilla* luciferase reporters.

(B) Dual-luciferase reporter assay showing that piRNAs promoted the activities of 3′ UTR reporters in GC-2spd (ts) cells, with mutated piRNAs serving as negative controls.

(C) qPCR assay showing that piRNAs barely altered the levels of 3′ UTR reporter mRNAs.

The average values ± SD of three separate experiments were plotted. *$p < 0.05$, **$p < 0.01$, ***$p < 0.001$, n.s., not significant. See also Figure S1.

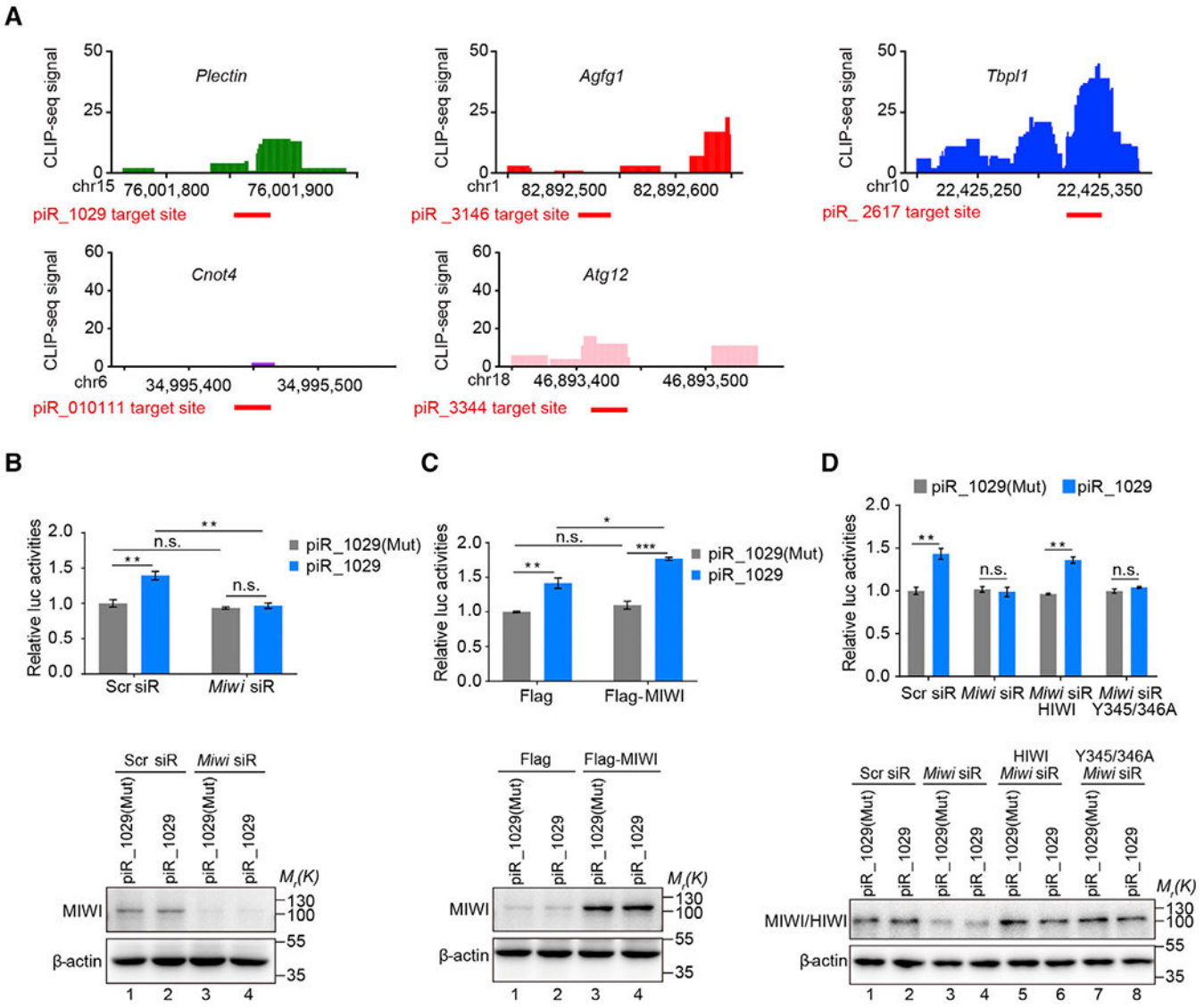

Figure 2. MIWI Is Essential for piRNA-Induced Target Activation

(A) Verification of piRNA target sites by MIWI crosslinking immunoprecipitation (CLIP) in mouse spermatids. Top: the cluster of MIWI CLIP tags on the five validated piRNA-activated genes, with the scales in genes numbered following the dimension of the chromosomes; bottom: the red thick lines indicate piRNA target sites.

(B and C) The effect of *Miwi* knockdown (B) or overexpression (C) on piR_1029-induced *Plectin* reporter activation in GC-2spd (ts) cells. Top: dual-luciferase reporter assay; bottom: western blotting assay of MIWI.

(D) Ectopic Flag-HIWI, but not its piRNA-loading-deficient Y345/346A mutant, rescued piR_1029-induced *Plectin* reporter activation in *Miwi* siR-treated GC-2spd(ts) cells. Top: dual-luciferase reporter assay; bottom: western blotting assay of MIWI or HIWI.

The average values ± SD of three separate experiments were plotted. *p < 0.05, **p < 0.01, ***p < 0.001, n.s., not significant. See also Figures S2A–S2D.

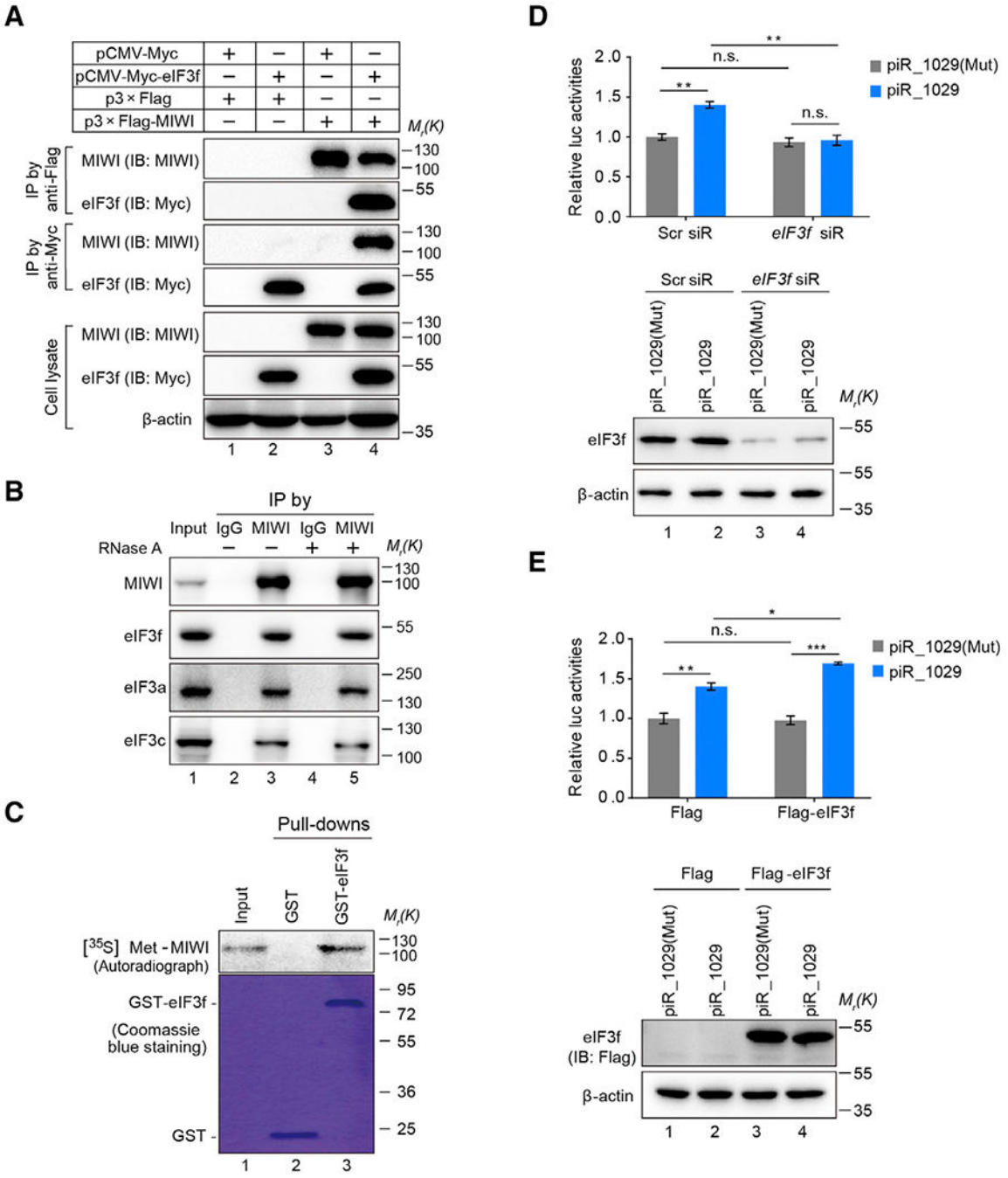

Figure 3. eIF3f, a MIWI-Interacting Protein, Is Required for piRNA-Induced Target Activation

(A and B) CoIP assay of MIWI-eIF3f interaction in Myc-eIF3f and Flag-MIWI co-transfected 293T cells (A) or adult mouse testes (B).

(C) GST pulldown assay showing a direct interaction between eIF3f and MIWI. Samples were analyzed by autoradiography (top) or visualized by Coomassie blue staining (bottom).

(D and E) The effect of *eIF3f* knockdown (D) or overexpression (E) on piR_1029-induced *Plectin* reporter activation in GC-2spd (ts) cells. Top: dual-luciferase reporter assay; bottom: western blotting assay of eIF3f.

The average values ± SD of three separate experiments were plotted. *$p < 0.05$, **$p < 0.01$, ***$p < 0.001$, n.s., not significant. See also Figures S2E–S2G and Table S1.

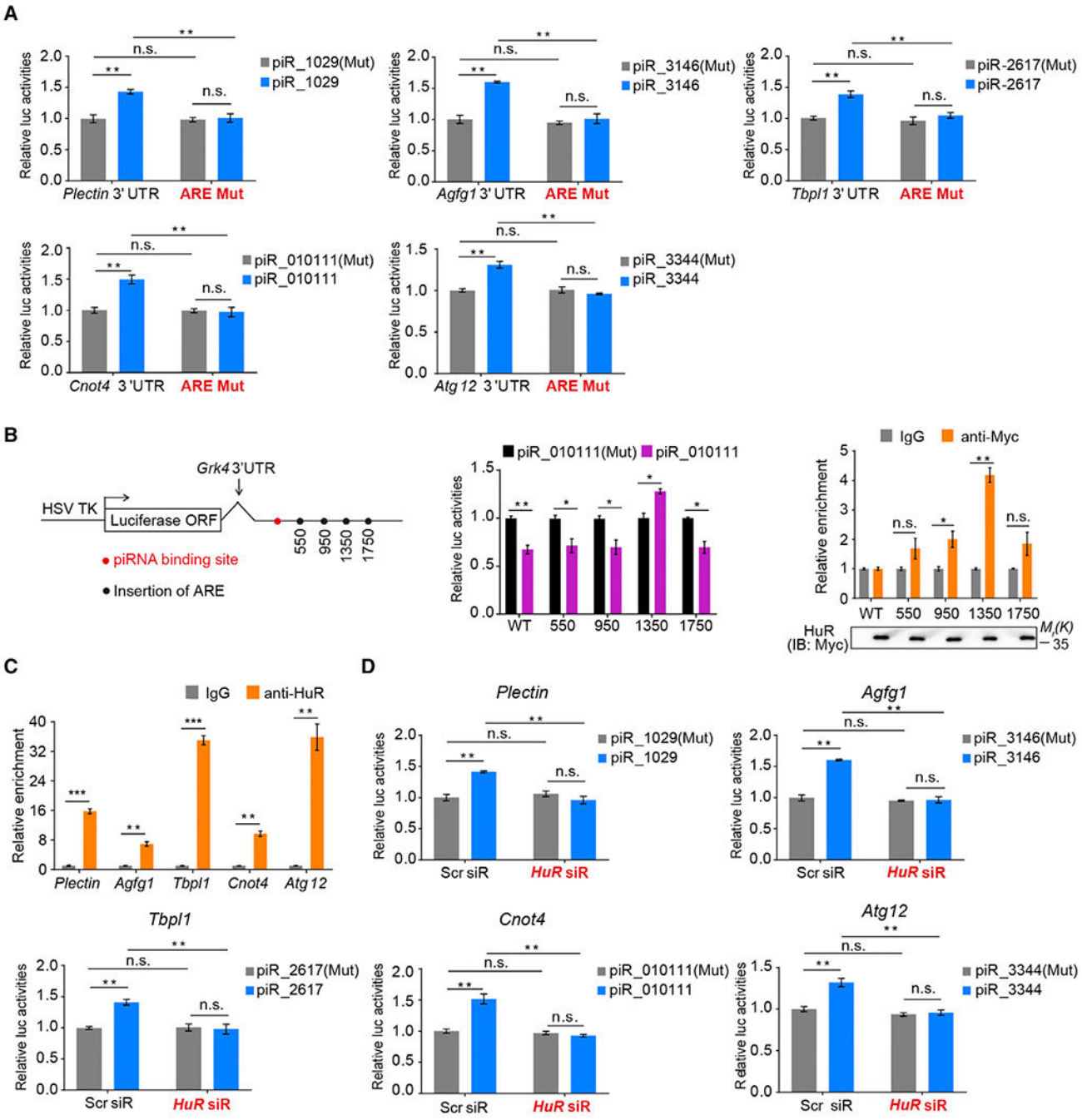

Figure 4. AREs in the 3′ UTRs of Target mRNAs Are Required for piRNA-Induced Target Activation

(A) Dual-luciferase reporter assay showing that deletion of AREs in target mRNAs impaired piRNA-induced target activation.

(B) Insertion of an ARE at position 1,350 nt downstream of piRNA-binding site reversed the repressive effect of piR_010111 to activation on the *Grk4* reporter in GC-2spd (ts) cells. Left: schematic diagram showing the position of piRNA-binding site (red spot) and respective ARE insertion (black spot) in *Grk4* reporter; middle: dual-luciferase reporter assay; right: RIP combined with qRT-PCR assays of HuR-binding to the ARE-containing

Grk4 reporter mRNAs, with relative enrichment of reporter mRNA in anti-HuR IP compared with IgG IP (top), using anti-HuR IB as loading references (bottom).

(C) RIP combined with qRT-PCR assays of HuR-binding to the five validated piRNA-activated mRNAs in mouse testes. Relative enrichment of indicated mRNA in HuR IP was compared with IgG IP.

(D) *HuR* knockdown substantially impaired the effect of piRNAs on the target reporters.

The average values ± SD of three separate experiments were plotted. *$p < 0.05$, **$p < 0.01$, ***$p < 0.001$, n.s., not significant. See also Figure S3 and Table S2.

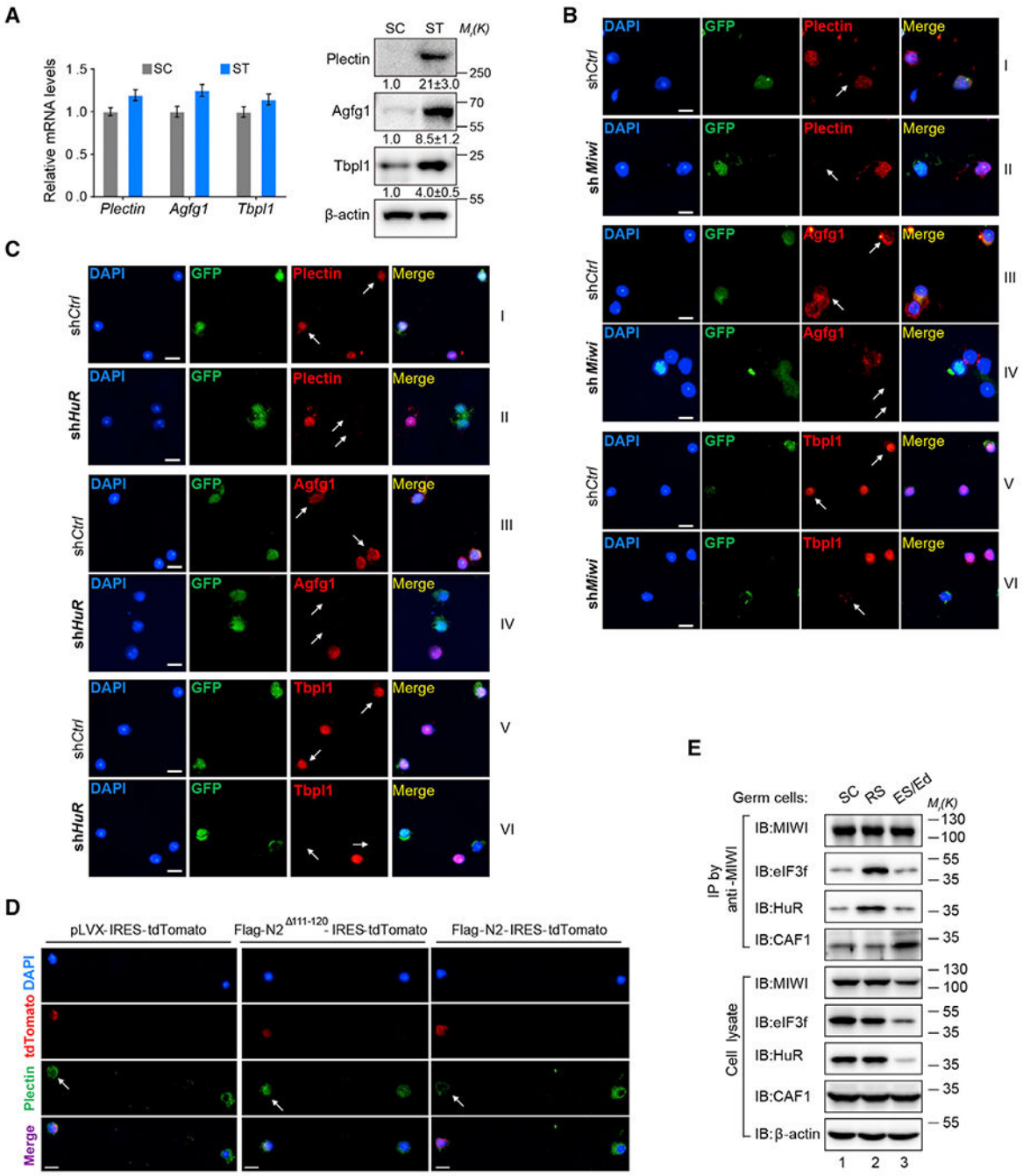

Figure 5. piRNA System Contributes to the Translation Activation Program in Mouse Spermatids

(A) qRT-PCR (left) and western blotting assays (right) of the expression of *Plectin, Agfg1*, and *Tbpl1* in enriched SCs and STs. Quantification of blotting intensity for indicated proteins is shown in parentheses (the one in SC is set as 1.0 after normalization with β-actin blotting).

(B and C) Immunofluorescent assay of the effect of *shMiwi*:GFP (B) or *shHuR*:GFP transduction (C) on Plectin (II), Agfg1 (IV), and Tbpl1 expression (VII) in mouse spermatids. GFP (green) and arrows indicate the transduced cells. Scale bar, 10 μm.

(D) Immunofluorescent assay of the effect of MIWI-N2 or MIWI-N2$^{\Delta 111–120}$ peptides on Plectin expression in control pLVX-IRES-tdTomato (left), Flag-MIWI-N2$^{\Delta 111–120}$ (middle), or Flag-MIWI-N2-transduced spermatids (right). tdTomato (red) and arrows indicate the transduced cells.

(E) CoIP assay of the association of MIWI with eIF3f, HuR, and CAF1 in SCs (lane 1), RSs (lane 2), and later stages of spermatids (ESs/elongated spermatids [Eds], lane 3).

Results shown are representative of three independent experiments. See also Figures S4, S5, and S6.

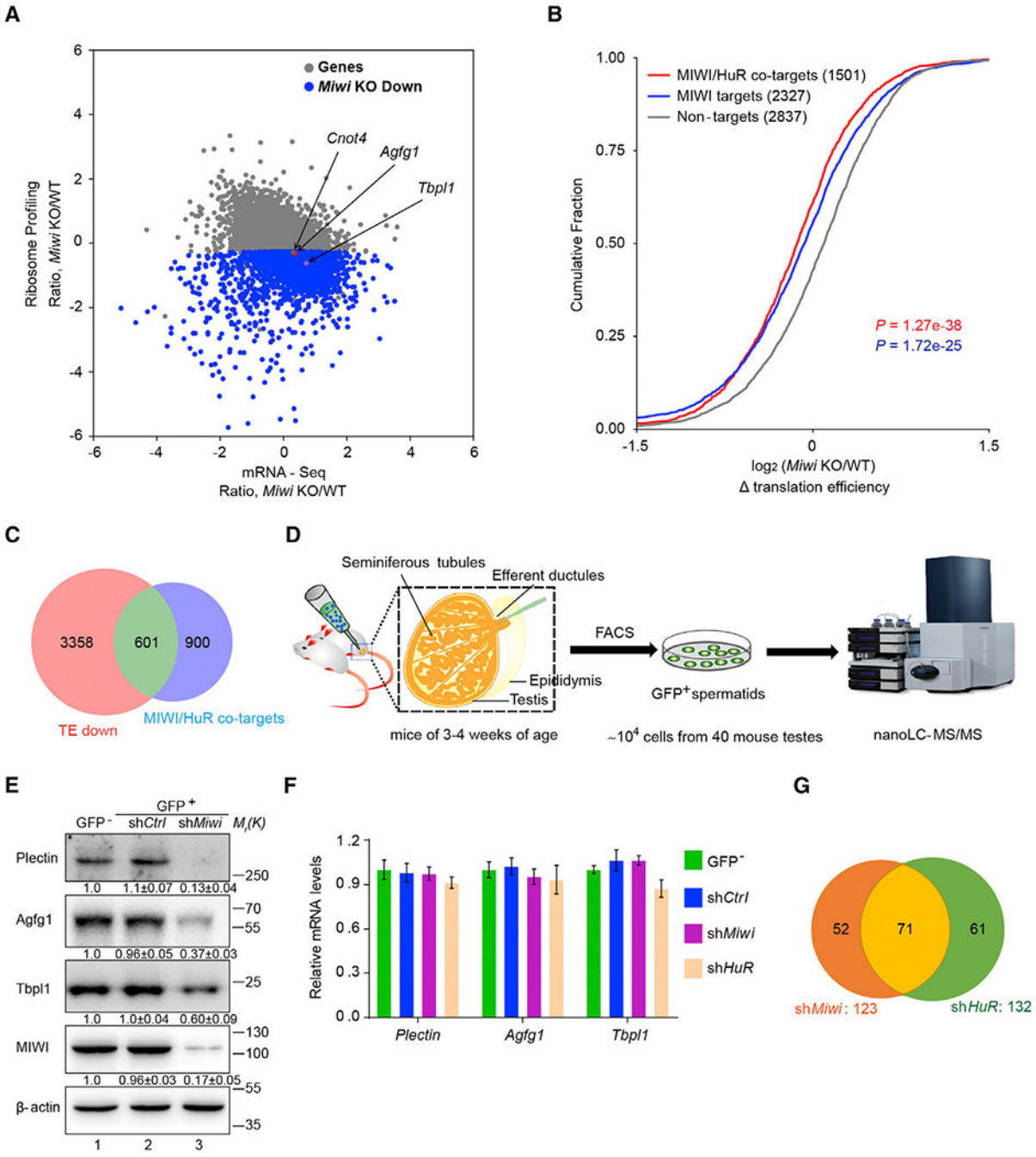

Figure 6. A Subset of Genes in Mouse Spermatids Is Subjected to Activation by the piRNA System

(A) Scatterplot showing mRNA level changes (x axis) against ribosome profiling changes (y axis) between *Miwi* null and wild-type testes. Arrows indicate the three validated piRNA-activated targets (i.e., *Agfg1, Tbpl1*, and *Cnot4*).

(B) Cumulative distribution of the log2-fold changes of translation efficiency (TE, ratio of ribosome-protected fragments [RPFs] and mRNA input) between the *Miwi* null and wild-type control samples for non-targets (no MIWI CLIP reads, gray line), MIWI targets (MIWI

CLIP peaks in 3′ UTRs, blue line), and MIWI/HuR co-targets (containing both MIWI and HuR-binding sites in 3′ UTRs, red line)

(C) Venn diagram showing the cross of MIWI/HuR co-target mRNAs (light blue) and translational efficiency-reduced mRNAs (TE down, pink) in *Miwi* null testes.

(D) Schematic diagram illustrating the experimental design.

(E) Western blotting assay of Plectin, Agfg1, and Tbpl1 expression in *sbMiwi*:GFP-transduced spermatids (lane 3), with quantification of blotting intensity shown in parentheses (the one in control GFP^- spermatids is set as 1.0 after normalization with β-actin blotting).

(F) qRT-PCR assay of the effect of *Miwi* or *HuR* knockdown on *Plectin, Agfg1*, and *Tbpl1* mRNA levels in mouse spermatids, with *β-actin* served as an internal control.

(G) Venn diagram representing the number of proteins that were downregulated (>2-fold) in *shMiwi*:GFP and *shHuR*:GFP-transduced spermatids compared with pSilencer:GFP control. Results shown are representative of three independent experiments. See also Figure S7 and Tables S3 and S4.

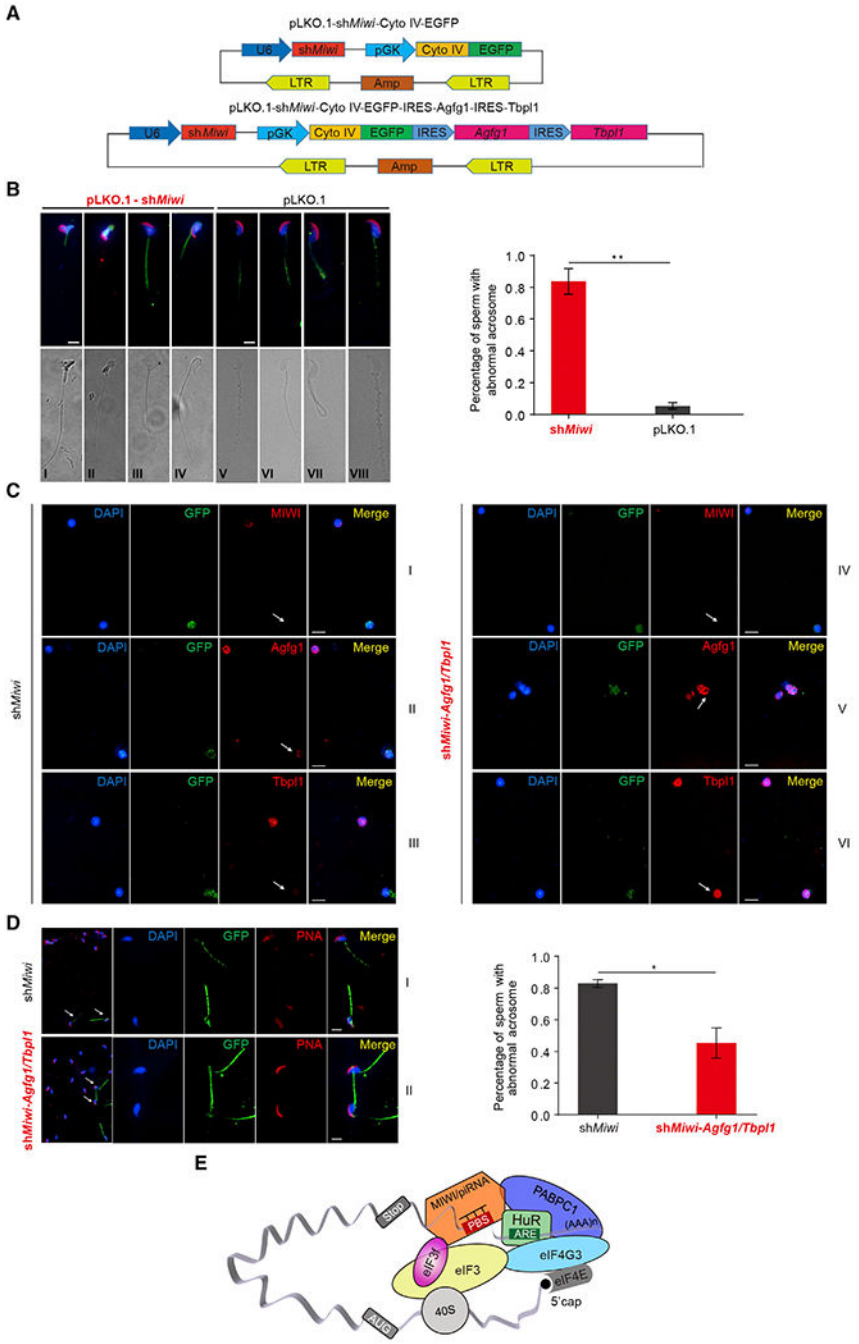

Figure 7. The piRNA System Is Required for Acrosome Formation during Spermiogenesis

(A) Schematic diagram showing the design of lentiviral shRNA vector pLKO.1-shRNA-Cyto IV-EGFP for *Miwi* knockdown (top) as well as co-expression of *shMiwi, Agfg1*, and *Tbpl1* (bottom). shRNA expression is driven by human U6 promoter, and Cyto IV (Cytochrome *c* oxidase subunit IV)-fused EGFP expression is driven by human phosphoglycerate kinase promoter (pGK). Cyto IV, a mitochondria-localized signal peptide; LTR, long terminal repeat; EGFP, enhanced green fluorescent protein; Amp, ampicillin resistance gene.

(B) Acrosome staining (Peanut agglutinin [PNA], red) of sperm progressed from *shMiwi* (left) or control shRNA-Cyto IV-EGFP-transduced spermatids (right), with nuclei counterstained by DAPI (blue). Left: representative PNA staining (top) and DIC micrograph images of GFP^+ sperm; right: percentages of GFP^+ sperm with abnormal acrosomes from indicated transduction (n = 100 per group). Scale bar, 10 μm.
(C) Immunofluorescent assay of MIWI (I and IV, red), Agfg1 (II or V, red) and Tbpl1 proteins (III and VI, red) in *shMiwi* (left) or *shMiwi*-Agfg/Tbpl1-transduced spermatids (right). GFP (green) indicates the transduced cells. Scale bar, 10 μm.
(D) Acrosome staining (red) of sperm progressed from *shMiwi* or *shMiwi*-Agfg1/Tbpl1-transduced spermatids (bottom), with nuclei counterstained by DAPI (blue). Left: representative PNA staining images of GFP^+ sperm; right: percentages of GFP^+ sperm with abnormal acrosomes from indicated transduction (n = 100 per group). Scale bar, 10 μm.
(E) Schematic model showing that MIWI/piRNA, eIF3f, and HuR cooperate to activate the translation of specific mRNAs in mouse spermatids. piRNAs guide MIWI to bind to the 3′ UTRs of ARE-containing target mRNAs and trigger mRNA looping through a direct interaction between MIWI and eIF3f; the mRNA looping is stabilized by ARE-guided HuR-binding to target mRNAs, thereby mediating the association of multiple other translation initiation factors, including eIF4G and PABPC1, to activate translation.
Results shown are representative of three independent experiments.

KEY RESOURCES TABLE

REAGENT or RESOURCE	SOURCE	IDENTIFIER
Antibodies		
Rabbit polyclonal anti-MIWI	This paper	Gou et al., 2014
Mouse monoclonal antibody anti-Flag	Sigma	Cat#F3165; RRID: AB_259529
Mouse monoclonal antibody anti-β-actin	Sigma	Cat#A3854; RRID: AB_262011
Rabbit polyclonal anti-c-Myc	Sigma	Cat#C3956; RRID: AB_439680
Mouse monoclonal antibody anti-HuR	Invitrogen	Cat#39-0600; RRID: AB_2533394
Mouse monoclonal antibody anti-GFP	Abways	Cat#AB0005
Mouse monoclonal antibody anti-AGO2	Abcam	Cat#ab57113; RRID: AB_2230916
Goat polyclonal anti-Mili	Santa Cruz	Cat#sc-67504;RRID: AB_2283941
Goat polyclonal anti-PIWIL1	Santa Cruz	Cat#sc-22685;RRID: AB_2165430
Goat polyclonal anti-Plectin	Santa Cruz	Cat#sc-7572; RRID: AB_654218
Rabbit polyclonal anti-Agfg1	Proteintech	Cat#12670-1-AP; RRID: AB_2258077
Rabbit polyclonal anti-Tbpl1	Proteintech	Cat#12258-1-AP; RRID: AB_10642841
Rabbit polyclonal anti-eIF3f	Abgent	Cat#AP2900a; RRID: AB_1967585
Rabbit polyclonal anti-eIF4G3	Novus	Cat#NBP2-16309
Rabbit polyclonal anti-GFP	MBL	Cat#598
Rabbit polyclonal anti-eIF3a	Bioworld	Cat#BS70526
Rabbit polyclonal anti-eIF3c	Bioworld	Cat#BS8653
Bacterial and Virus Strains		
TOP10 chemically competent *E.coli*	TIANGEN	CB104
BL21 chemically competent *E.coli*	TIANGEN	CB105
Chemicals, Peptides, and Recombinant Proteins		
Cycloheximide	MCE	HY-12320
Turbo DNase	Invitrogen	AM2238
SUPERase·In	Invitrogen	AM2694
GST-eIF3f	This paper	N/A
Critical Commercial Assays		
Lipofectamine 2000	ThermoFisher	11668019
Lipofectamine 3000	ThermoFisher	L3000015
RNAiso Plus	Takara	9109
PrimeScript RT reagent Kit with gDNA Eraser	Takara	RR047A
SYBR Premix Ex Taq II	Takara	RR820A
Deposited Data		
Elongating spermatids CLIP-seq data	Gou et al., 2014	SRP043638
Round spermatids CLIP-seq data	Zhang et al., 2015	GSE67683
Ribosome profiling	This paper	GSE139399
Experimental Models: Cell Lines		

REAGENT or RESOURCE	SOURCE	IDENTIFIER
Human: 293T	ATCC	CRL-3216
Mouse: GC-2spd (ts)	ATCC	CRL-2196
Experimental Models: Organisms/Strains		
C57BL6 male mice	SLAC	N/A
B6.129-*Piwil1*^{1Hfl}/Mmmh	MMRRC	29995
Oligonucleotides		
Sequences for qPCR Primers, see Table S5	This paper	N/A
Sequences for shRNA primers, see Table S5	This paper	N/A
Sequences for piRNAs, see Table S6	This paper	N/A
Sequences for siRNAs, see Table S6	This paper	N/A
Recombinant DNA		
pRL-TK	Promega	E2241
pRL-TK-Plectin-3′ UTR	This paper	N/A
pRL-TK-Agfg1-3′ UTR	This paper	N/A
pRL-TK-Tbpl1-3′ UTR	This paper	N/A
pRL-TK-Cnot4-3′ UTR	This paper	N/A
pRL-TK-Atg12-3′ UTR	This paper	N/A
pGL3	Promega	E1761
p3xFLAG-CMV™-10	Sigma	E7658
p3xFLAG-CMV™-10-MIWI	This paper	N/A
p3xFLAG-CMV™-10-HIWI	This paper	N/A
p3xFLAG-CMV™-10-HIWI-Y345/346A	This paper	N/A
p3xFLAG-CMV™-10-eIF3f	This paper	N/A
pCMV-Myc	Clontech	631604
pCMV-Myc-eIF3f	This paper	N/A
pCMV-Myc-HuR	This paper	N/A
pCMV-Myc-PABPC1	This paper	N/A
pCMV-Myc-PABPC2	This paper	N/A
pGEX-KG	ATCC	77103
pGEX-KG-eIF3f	This paper	N/A
pSilencer-H1	N/A	N/A
pSilencer-H1-*shMiwi*	This paper	N/A
pSilencer-H1-*shHuR*	This paper	N/A
pLKO.1	Addgene	N/A
pLKO.1-Cyto IV-EGFP	This paper	N/A
pLKO.1-*shMiwi*-CytoIV-EGFP	This paper	N/A
pLKO.1-*shHuR*-CytoIV-EGFP	This paper	N/A
pLKO.1-*shMiwi*-CytoIV-EGFP-IRES-Agfg1-IRES-Tbpl1	This paper	N/A
p3xFLAG-CMV-10-MIWI-N	This paper	N/A

REAGENT or RESOURCE	SOURCE	IDENTIFIER
p3xFLAG-CMV-10-MIWI-PAZ+MID	This paper	N/A
p3xFLAG-CMV-10-MIWI-PIWI	This paper	N/A
p3xFLAG-CMV-10-MIWI-N1	This paper	N/A
p3xFLAG-CMV-10-MIWI-N2	This paper	N/A
p3xFLAG-CMV-10-MIWI-N3	This paper	N/A
p3xFLAG-CMV-10-MIWI-N4	This paper	N/A
p3xFLAG-CMV-10-MIWI-N2$^{\Delta 111–120}$	This paper	N/A
p3xFLAG-CMV-10-eIF4G3	This paper	N/A
pLVX-IRES-tdTomato	Clontech	631238
pLVX-FLAG-MIWI-N2-IRES-tdTomato	This paper	N/A
pLVX-FLAG-MIWI-N2$^{\Delta 111–120}$-IREStdTomato	This paper	N/A
Software and Algorithms		
GraphPad Prism	GraphPad	N/A
Photoshop CS3	Adobe	N/A
ImageJ	NIH	https://imagej.nih.gov/ij/